Physica B 405 (2010) 1927–1940

Contents lists available at ScienceDirect

Physica B

journal homepage: www.elsevier.com/locate/physb

Reanalysis of energy levels and crystal field parameters for Er^{3+} and Tm^{3+} ions at C_2 symmetry sites in hexahydrated trichloride crystals—Intricate aspects of multiple solutions for monoclinic symmetry

M. Karbowiak [a,*], P. Gnutek [b], C. Rudowicz [b]

[a] Faculty of Chemistry, University of Wrocław, ul. F. Joliot-Curie 14, 50-383 Wrocław, Poland
[b] Modeling in Spectroscopy Group, Institute of Physics, West Pomeranian University of Technology, Al. Piastów 17, 70-310 Szczecin, Poland

ARTICLE INFO

Article history:
Received 7 January 2010
Accepted 13 January 2010

Keywords:
Energy levels
Low-symmetry
Crystal-field
Hexahydrated lanthanide trichlorides

ABSTRACT

Crystal-field splittings of lanthanide Ln^{3+} (Ln=Er, Tm) ions in hexahydrated Ln-trichlorides $LnCl_3 \cdot 6H_2O$ are re-analyzed in order to obtain consistent and standardized crystal-field parameter (CFP) sets. Experimental energy levels obtained by others were fitted to Hamiltonian parameters representing the combined free-ion and crystal-field interactions for Er^{3+} and Tm^{3+} ions in the actual monoclinic C_2 symmetry sites. The reliable starting values of the CFPs were obtained from superposition model calculations. Analysis of multiple solutions with relatively low *r.m.s.* deviation poses a dilemma arising from intricate aspects of fitted CFPs for low site symmetry systems. In order to solve this dilemma we propose a comprehensive procedure consisting in (i) model calculations of CFPs, (ii) scanning of the CF parameter space using values of the starting 2nd-rank CFPs in reasonable ranges, (iii) using starting CFP sets located in different regions of the CF parameter space for fittings, (iv) considering the effect of sign changes in CFPs on the fitted solutions, and (v) comparative analysis of the transformation properties of all fitted CFP sets based on the monoclinic standardization approach and the multiple correlated fitting technique. An important finding is that some of the multiple and *seemingly* comparable solutions for fitted CFP sets turn out to be spurious solutions. The nature of these computer artifacts is elucidated. Such artifacts occur when the descent in symmetry method is applied for initial evaluation of the starting CFPs, while the approximated higher symmetry axes do not coincide with the actual symmetry axes. Wider applications of the proposed procedure in CF studies of low site symmetry systems may improve the reliability of the CFP sets reported in literature.

© 2010 Elsevier B.V. All rights reserved.

1. Introduction

The hexahydrated lanthanide (Ln) trichlorides $LnCl_3 \cdot 6H_2O$ have served as one of the first crystalline hosts for studies of spectroscopic properties of the trivalent Ln^{3+} ions [1,2] since the late 60s. Theoretical investigations of the crystal-field (CF) energy levels of Ln^{3+} ions were carried out within the parametric Hamiltonian framework [1] assuming the actual monoclinic C_2 site symmetry for $ErCl_3 \cdot 6H_2O$ [3], $HoCl_3 \cdot 6H_2O$ [4] and $TmCl_3 \cdot 6H_2O$ [5]. Coture and Rajnak [6] presented an extended set of experimental energy levels for Er^{3+} in $ErCl_3 \cdot 6H_2O$, obtained from optical spectra recorded for crystals and frozen aqueous solutions, and interpreted them using the approximate D_{4d} symmetry. Similarly, higher orthorhombic C_{2v} approximation instead of C_2 symmetry, was employed in the CF analysis of absorption and magnetic circular dichroism spectra of polycrystalline $EuCl_3 \cdot 6H_2O$ [7]. Experimental energy levels of $GdCl_3 \cdot 6H_2O$ were reported in Ref. [8]; however, their analysis based on a free-ion Hamiltonian was limited to the center of gravity of SLJ multiplets.

In our previous paper [9] we presented preliminary results of CF analysis for Ho^{3+} ions in $HoCl_3 \cdot 6H_2O$. Our motivation for re-analysis of CF splittings of Ln^{3+} ions in $LaCl_3 \cdot 6H_2O$ stems primarily from two aspects: (i) existence in literature of the non-standard (as defined in [10]) CF parameters (CFPs), which hinders their direct comparison [11], and (ii) usage of some faulty procedures in determination of the starting CFP values for Ho^{3+} [4] and Tm^{3+} [5] in hexahydrated chlorides indicated in Ref. [10], which may be a possible reason that the results of parametric fittings for $ErCl_3 \cdot 6H_2O$ [3] and $TmCl_3 \cdot 6H_2O$ [5] do not represent the best (global) minima. Our trial simulations using random numbers as the starting CFPs yield, in <10 trials, solutions with lower *r.m.s.* values than those reported in Refs. [3,5]. Hence, it seems worthwhile to provide standardized CFP sets and reconsider earlier CF analysis [3–6].

Besides, $LnCl_3 \cdot 6H_2O$ are good model systems for elucidating low symmetry aspects, which seem not to be generally recognized in CF studies as yet. $LnCl_3 \cdot 6H_2O$ belong to relatively small group

* Corresponding author. Tel.: +48 71 375 7304; fax: +48 71 328 2348.
E-mail address: karb@wchuwr.pl (M. Karbowiak).

0921-4526/$ - see front matter © 2010 Elsevier B.V. All rights reserved.
doi:10.1016/j.physb.2010.01.086

of lanthanide compounds for which a comprehensive number of energy levels was experimentally determined and assigned. Their crystal structure is well established and the monoclinic symmetry axis is well-defined. Moreover, for $TmCl_3 \cdot 6H_2O$ the direction of magnetization axis with respect to the crystallographic axis system (CAS) is known [12], which enables additional correlation of the axis system (AS) chosen for the CF analysis with the crystallographic structure.

In this paper we present results of reanalysis of energy levels and CFPs for Er^{3+} and Tm^{3+} ions at C_2 symmetry sites in hexahydrated trichloride crystals. It is generally accepted that CFP modeling, analysis and fitting are increasingly difficult and potentially unreliable for low site symmetry ion-host systems. Fitting of monoclinic and triclinic CFPs is especially prone to misinterpretations as indicated by the discrepancies between results obtained by various authors for the same or structurally similar systems, see, e.g. in Refs. [13–16]. Hence, it would be helpful to set clear criteria, e.g. on how to analyze fitted CFPs, distinguish between numerically comparable fitted solutions which may be physically inequivalent, make selection of final CFP sets, and correlate fitted CFP sets with well-defined axes in crystals. The major aim of this paper is to provide such criteria based the case studies of Ln^{3+} ions in $LnCl_3 \cdot 6H_2O$. Hence, we propose a comprehensive procedure consisting in (i) model calculations of CFPs, (ii) scanning of the CF parameter space using values of the starting 2nd-rank CFPs in reasonable ranges, (iii) using starting CFP sets located in different regions of the CF parameter space for fittings, (iv) considering the effect of sign changes in CFPs on the fitted solutions, and (v) comparative analysis of the transformation properties of all fitted CFP sets based on the monoclinic standardization approach and the multiple correlated fitting technique [10,11].

Our CF analysis yields better minima than previously reported and indicates that 2nd-rank starting CFPs may have a decisive influence on the region in the multidimensional CF parameters space, in which the final solutions are obtained. An important finding is that among the multiple, *seemingly* comparable, solutions for the fitted CFP sets, some sets correspond to the *nominal* axis systems (as defined in Ref. [11]) with the *x*- or *y*-axis *apparently* parallel to the monoclinic axis, even if the starting CFPs were expressed in the axis system with the *z*-axis taken along the monoclinic axis. Importantly, it turns out that such *apparently* correlated fitted solutions cannot be transformed one into another, which indicates that two out of three such solutions must represent computer artifacts. Question arises what criteria can help us to find out the spurious solutions. This dilemma is solved by the proposed careful comparative analysis of the fitted CFP sets. We also show that, although consideration of the approximated higher symmetry may be useful for CF analysis of ion-host systems exhibiting lower site symmetry, the descent in symmetry method may lead to spurious solutions. This may happen if not enough care is paid to the transformation properties of CFPs expressed in the axis systems corresponding to the higher and actual site symmetry.

Our study elucidates intricate aspects of multiple solutions for fitted CFPs, which are inherent in CF calculations for low site symmetry systems. A survey of literature reveals that these aspects and their implications have not been recognized in the up-to-now studies. Inadvertent disregarding of the aspects in question may lead to serious pitfalls, as exemplified by the case studies considered in details here. Greater awareness of these problems should help avoiding such pitfalls in future CF studies, thus increasing reliability of the final CFP sets. Our considerations may be very helpful in future CF analysis for low site symmetry ion-host systems.

2. Theory

For the energy level calculations we apply the effective operator model suitable for $4f^N$ ions in crystals [1,17,18]. The observed energy levels are fitted to the phenomenological Hamiltonian, $\hat{H} = \hat{H}_{FI} + \hat{H}_{CF}$, by simultaneous diagonalization of the free-ion ($\hat{H}_{FI}$) Hamiltonian:

$$\hat{H}_{FI} = E_{ave} + \sum_{k=2,4,6} F^k(nf,nf)\hat{f}_k + \zeta_{5f}\hat{A}_{SO} + \alpha\hat{L}(\hat{L}+1) + \beta\hat{G}(G_2) + \gamma\hat{G}(R_7) + \sum_{i=2,3,4,6,7,8} T^i\hat{t}_i + \sum_{j=0,2,4} M^j\hat{m}_j + \sum_{k=2,4,6} P^k\hat{p}_k, \quad (1)$$

and the crystal field Hamiltonian ($\hat{H}_{CF}$):

$$\hat{H}_{CF} = \sum_{k,q} B_{kq}\hat{C}_q^{(k)}(x,y,z). \quad (2)$$

The operators and interaction parameters in Eq. (1) as well as the intra-configurational spherical-tensor operators $\hat{C}_q^{(k)}$, expressed in a given axis system (*x*,*y*,*z*), and CFPs B_{kq}, of rank *k* and component *q*, in Eq. (2) are defined according to the conventional practice [1,17]. The relation holds $B_{k-q} = (-1)^q B_{kq}^*$ and thus B_{kq} may be represented as $B_{kq} = \mathrm{Re}\,B_{kq} + i\mathrm{Im}\,B_{kq}$, see, e.g. [19].

For monoclinic (C_2, C_S, C_{2h}) symmetry sites, where only one symmetry axis C_2 (or direction) exists, the most common choice of the *z*-axis in Eq. (2) as parallel to the monoclinic C_2 axis ($C_2||z$) yields

$$\begin{aligned}\hat{H}_{CF} = {} & B_{20}\hat{C}_0^2 + \mathrm{Re}\,B_{22}(\hat{C}_{-2}^2 + \hat{C}_2^2) + \mathrm{Im}\,B_{22}(\hat{C}_{-2}^2 - \hat{C}_2^2) + B_{40}\hat{C}_0^4 \\ & + \mathrm{Re}\,B_{42}(\hat{C}_{-2}^4 + \hat{C}_2^4) + \mathrm{Im}\,B_{42}(\hat{C}_{-2}^4 - \hat{C}_2^4) + \mathrm{Re}\,B_{44}(\hat{C}_{-4}^4 + \hat{C}_4^4) \\ & + \mathrm{Im}\,B_{44}(\hat{C}_{-4}^4 - \hat{C}_4^4) + B_{60}\hat{C}_0^6 + \mathrm{Re}\,B_{62}(\hat{C}_{-2}^6 + \hat{C}_2^6) \\ & + \mathrm{Im}\,B_{62}(\hat{C}_{-2}^6 - \hat{C}_2^6) + \mathrm{Re}\,B_{64}(\hat{C}_{-4}^6 + \hat{C}_4^6) + \mathrm{Im}\,B_{64}(\hat{C}_{-4}^6 - \hat{C}_4^6) \\ & + \mathrm{Re}\,B_{66}(\hat{C}_{-6}^6 + \hat{C}_6^6) + \mathrm{Im}\,B_{66}(\hat{C}_{-6}^6 - \hat{C}_6^6). \end{aligned} \quad (3)$$

Besides the choice $C_2||z$, two other choices of the axis system (*x*,*y*,*z*) in Eq. (2) exist, i.e. $C_2||x$ and $C_2||y$. The two alternative choices correspond to transformation of the original (*x*,*y*,*z*) axes to (*y*,*z*,*x*) and (*z*,*x*,*y*) and yield different forms of the $\hat{H}_{CF}$, respectively,

$$\begin{aligned}\hat{H}_{CF} = {} & B_{20}\hat{C}_0^2 + \mathrm{Im}\,B_{21}(\hat{C}_{-1}^2 + \hat{C}_1^2) + \mathrm{Re}\,B_{22}(\hat{C}_{-2}^2 + \hat{C}_2^2) + B_{40}\hat{C}_0^4 \\ & + \mathrm{Im}\,B_{41}(\hat{C}_{-1}^4 + \hat{C}_1^4) + \mathrm{Re}\,B_{42}(\hat{C}_{-2}^4 + \hat{C}_2^4) + \mathrm{Im}\,B_{43}(\hat{C}_{-3}^4 + \hat{C}_3^4) \\ & + \mathrm{Re}\,B_{44}(\hat{C}_{-4}^4 + \hat{C}_4^4) + B_{60}\hat{C}_0^6 + \mathrm{Im}\,B_{61}(\hat{C}_{-1}^6 + \hat{C}_1^6) \\ & + \mathrm{Re}\,B_{62}(\hat{C}_{-2}^6 + \hat{C}_2^6) + \mathrm{Im}\,B_{63}(\hat{C}_{-3}^6 + \hat{C}_3^6) + \mathrm{Re}B_{64}(\hat{C}_{-4}^6 + \hat{C}_4^6) \\ & + \mathrm{Im}\,B_{65}(\hat{C}_{-5}^6 + \hat{C}_5^6) + \mathrm{Re}\,B_{66}(\hat{C}_{-6}^6 + \hat{C}_6^6), \end{aligned} \quad (4)$$

$$\begin{aligned}\hat{H}_{CF} = {} & B_{20}\hat{C}_0^2 + \mathrm{Re}\,B_{21}(\hat{C}_{-1}^2 - \hat{C}_1^2) + \mathrm{Re}\,B_{22}(\hat{C}_{-2}^2 + \hat{C}_2^2) + B_{40}\hat{C}_0^4 \\ & + \mathrm{Re}\,B_{41}(\hat{C}_{-1}^4 - \hat{C}_1^4) + \mathrm{Re}\,B_{42}(\hat{C}_{-2}^4 + \hat{C}_2^4) + \mathrm{Re}\,B_{43}(\hat{C}_{-3}^4 - \hat{C}_3^4) \\ & + \mathrm{Re}\,B_{44}(\hat{C}_{-4}^4 + \hat{C}_4^4) + B_{60}\hat{C}_0^6 + \mathrm{Re}\,B_{61}(\hat{C}_{-1}^6 - \hat{C}_1^6) \\ & + \mathrm{Re}\,B_{62}(\hat{C}_{-2}^6 + \hat{C}_2^6) + \mathrm{Re}\,B_{63}(\hat{C}_{-3}^6 - \hat{C}_3^6) + \mathrm{Re}\,B_{64}(\hat{C}_{-4}^6 + \hat{C}_4^6) \\ & + \mathrm{Re}\,B_{65}(\hat{C}_{-5}^6 - \hat{C}_5^6) + \mathrm{Re}\,B_{66}(\hat{C}_{-6}^6 + \hat{C}_6^6). \end{aligned} \quad (5)$$

Explicit forms of the $\hat{H}_{CF}$ in Eqs. (3)–(5) will be useful in the comprehensive procedure proposed below.

After reducing all respective monoclinic CFP to zero in Eqs. (3)–(5), we obtain the orthorhombic $\hat{H}_{CF}$ form, which is invariant with respect to the axis systems chosen; however, the values of CFPs would change in each case. For orthorhombic CFPs the value of the *rhombicity* ratio κ defined as [10,11]

$$\kappa = \mathrm{Re}\,B_{22}/B_{20}, \quad (6)$$

is a crucial quantity that determines intricate properties of CFP sets. It is worth to mention that fittings of the experimental

energy levels using any of the three $\hat{H}_{CF}$ forms in Eqs. (3)–(5) may yield, after reducing the respective monoclinic 2nd-rank CFP to zero, the value of κ in Eq. (6) anywhere between $+\infty$ and $-\infty$ depending, to a great extent, on the region to which the starting CFPs belong. What is important is that specific fitted CFP sets may form groups of the alternative correlated and physically equivalent sets [10,11]. Hence, possible correlations between CFP sets must be carefully explored in order to identify such CFP groups. Method to achieve this goal and practical examples are considered in Section 3.

To facilitate comparison of CFP sets obtained by various authors employing different methods, the CF strength parameters [20] S_k (k=2, 4, 6) and S, which are rotationally invariant quantities [21], are used:

$$S_k = [(2k+1)^{-1}\left((B_{ko})^2 + 2\sum_{q>0}((\mathrm{Re}\,B_{kq})^2 + (\mathrm{Im}\,B_{kq})^2)\right)]^{1/2},$$
$$S = [(1/3)\sum_k S_k^2]^{1/2}. \quad (7)$$

The starting values of CFPs for fittings may be estimated using the superposition model (SPM) expression [14,22]

$$B_{kq} = \sum_L \overline{B}_k(R_L) g_{k,q}(\theta_L, \varphi_L), \quad (8)$$

where $\overline{B}_k$ are the intrinsic parameters and $g_{k,q}$ are the coordination factors. The main SPM assumption is that the CFPs for a central metal ion may be expressed as a sum of cylindrically symmetric single-ligand (L) contributions [14].

3. Results and discussion

3.1. Energy level calculations and fittings of free-ion and CFPs for Er^{3+} ions in $ErCl_3 \cdot 6H_2O$

The Er^{3+} ions occupy C_2 symmetry sites and the C_2 axis is parallel to the crystallographic b-axis. The nearest neighborhood of the erbium central ion is formed by two chlorine anions lying at distance 273.0 pm and three groups of oxygen atoms lying at distance 233.1, 237.4 and 238.8 pm. $ErCl_3 \cdot 6H_2O$ crystallizes in the monoclinic P2/n space group. This necessitates adoption of a modified (Cartesian) crystallographic axis system (CAS*) instead of the original non-Cartesian CAS (a,b,c). In SPM calculations of $g_{k,q}$ we chose the axis system (x,y,z) so that the C_2 axis, directed along the crystallographic b-axis, coincides with the z-axis and both Cl ligands are placed along the x-axis, whereas the angle between the Cartesian y-axis and the crystallographic a-axis is equal to 6.005°. Ligand positions corresponding to this choice of the CAS*: ($a^*||y$, $b||C_2||z$, $c||x$) are listed in Table 1 of Ref. [9], whereas relative orientations of the axes (x,y,z), (a,b,c), and (a^*,b,c) are depicted in Fig. 1.

Table 1
CF parameters for Er^{3+} ions in $ErCl_3 \cdot 6H_2O$ obtained from the energy level data [6] using various fitting and transformation approaches together with the respective $\hat{H}_{CF}$ form represented by a given (fitted or transformed) CFP set.

Set $\hat{H}_{CF}$ form	*Er-SPM* $C_2\|\|z$	*Er-I-Fit-C* $C_2\|\|z$	*Er-I-Fit-R*[a] $C_2\|\|z$	*Er-II-Fit-R*[b] $C_2\|\|z$	*Er-III-Fit-R*[b] $C_2\|\|z$	*Er-I-ST* $C_2\|\|x$	*Er-II-ST* $C_2\|\|y$	*Er-III-ST* $C_2\|\|z$
B_{20}	194	170	170	335	−513	−513	−512	−513
ReB_{21}	–	–	–	–	–	–	0	–
ImB_{21}	–	–	–	–	–	0	–	–
ReB_{22}	−108	−252	−349	−282	62	−71	−64	−62
ImB_{22}	−323	−242	[0]	[0]	[0]	–		–
κ	–	–	−2.05	−0.84	−0.12	0.14	0.12	0.12
B_{40}	−458	−360	−360	−352	−1041	−1034	−1031	−1041
ReB_{41}	–	–	–	–	–	–	−180	–
ImB_{41}	–	–	–	–	–	158	–	–
ReB_{42}	118	303	451	382	−46	24	48	46
ImB_{42}	427	335	32	129	−46	–	–	−46
ReB_{43}	–	–	–	–	–	–	−70	–
ImB_{43}	–	–	–	–	–	26	–	–
ReB_{44}	228	136	−519	−571	67	45	−3	67
ImB_{44}	−442	−525	−158	−144	−89	–	–	89
B_{60}	−20	−201	−201	52	552	521	539	552
ReB_{61}	–	–	–	–	–	–	125	–
ImB_{61}	–	–	–	–	–	−152	–	–
ReB_{62}	−12	71	182	110	260	−163	−184	−260
ImB_{62}	242	188	87	306	92	–	–	92
ReB_{63}	–	–	–	–	–	–	159	–
ImB_{63}	–	–	–	–	–	−170	–	–
ReB_{64}	−82	−177	−370	−189	−129	−177	−59	−129
ImB_{64}	−255	−363	162	−23	−159	–	–	159
ReB_{65}	–	–	–	–	–	–	239	–
ImB_{65}	–	–	–	–	–	−190	–	–
ReB_{66}	−375	−232	86	371	85	−61	−65	−85
ImB_{66}	−1	−89	233	62	98	–	–	98
S_2	232	234	234	233	233	234	233	233
S_4	349	354	354	356	352	354	356	352
S_6	204	210	210	209	210	210	209	210
S	269	273	273	274	272	273	274	272
r.m.s.	–	14.1	14.0	14.2	14.7	–	–	–

For explanations see text.

[a] For this fit the free-ion parameters were determined as (all values in cm^{-1}): E_{avg}=35711(2), F^2=96869(16), F^4=67842(39), F^6=55715(26), and ζ_{4f}=2380(1), while other parameters were kept constant as follows [6]: α=19.17, β=−611.0, γ=1571, T^2=518, T^3=34, T^4=76, T^6=−340, T^7=317, T^8=393, M^0=4.58, M^2=2.56, M^4=1.74, P^2=740, P^4=555, P^6=370. For other fitted CFP sets practically the same free-ion parameters were obtained within the uncertainties for the respective parameters, so we refrain from listing them here.

[b] Sets transformed from the fitted sets *Er-X-Fit-C* by reduction of ImB_{22} to zero.

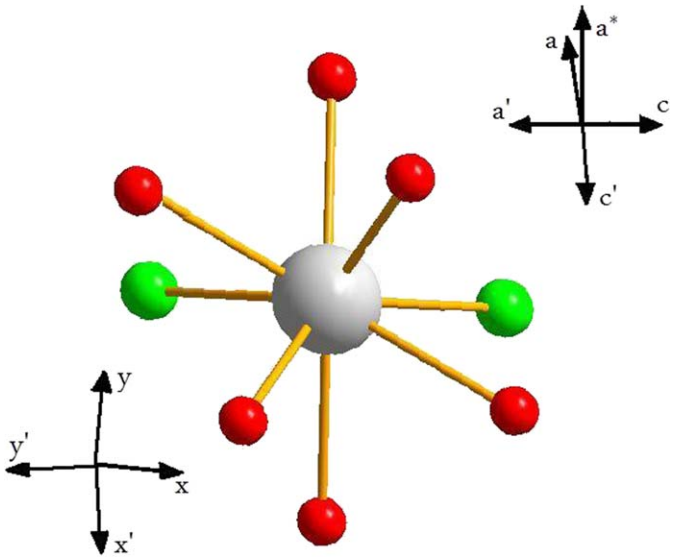

Fig. 1. Relative orientation of the crystallographic axis system (CAS) (a,b,c) for $ErCl_3 \cdot 6H_2O$ [24], the modified Cartesian CAS* (a^*,b,c), and the axis system (x,y,z) chosen for SPM calculations. The monoclinic C_2 axis is parallel to the crystallographic b-axis. The axis (a',b',c') reported in Ref. [23] for $GdCl_3 \cdot 6H_2O$ as well as the axis system (x',y',z') used by Olsen et al. [5] are also depicted.

Harrop [3] and Olsen et al. [5] used in their CF calculations the crystallographic data reported in Ref. [23] for $GdCl_3 \cdot 6H_2O$. In their axis system (x',y',z'), the crystallographic b'-axis coincides with the z'-axis, whereas the x'-axis is parallel to the c'-axis. The angle between the y'- and a'-axis is equal to 3.64°. Note, however, that the convention for the crystallographic axes (a,b,c) used in Ref. [24] for $ErCl_3 \cdot 6H_2O$ differs from that for the axes (a',b',c') in Ref. [23] for $GdCl_3 \cdot 6H_2O$; the relation holds (a,b,c)→($-c'$,b',$-a'$). The relative orientations of the crystallographic axes (a,b,c) [24] and (a',b',c') [23], and the axis system (x',y',z') used by Olsen et al. [5] with respect to our axes (x,y,z) are also indicated in Fig. 1.

In the first step, we carried out the SPM calculations of CFPs, which required a total of 12 intrinsic parameters for the systems under investigation. Crystallographic data available for $ErCl_3 \cdot 6H_2O$ [24] and the spherical polar expressions [14] for the coordination factors $g_{k,q}$ in Eq. (8) were used in our calculations. If the power exponents t_k were known the number of parameters could be reduced using the relation $\overline{B}_k(R_L) = \overline{B}_k(R_0)(R_0/R_L)^{t_k}$, where R_0 is the reference ligand distance [14]. However, since the distance dependence of the intrinsic parameters for water oxygen is unknown, we assume the clustered distance approximation [22], i.e. all oxygen ligands are grouped into one set with the average Er–O distance equal to 236.4 pm. This yields six intrinsic parameters, which were optimized by fitting to experimental data. In our CF analysis we employ the experimental CF splittings for Er^{3+} in $ErCl_3 \cdot 6H_2O$ taken from Table 1 of Ref. [6], which encompasses 120 energy levels. The fit, in which the free-ion parameters (E_{avg}, F^2, F^4, F^6, and ζ_{4f}) were also freely varied, yields the intrinsic parameters (in cm^{-1}): $\overline{B}_2$ (Cl)=1234 ± 37, $\overline{B}_4$ (Cl)=156 ± 69, $\overline{B}_6$ (Cl)=185 ± 56, and $\overline{B}_2$ (O)=1026 ± 25, $\overline{B}_4$ (O)=478 ± 28, $\overline{B}_6$ (O)=321 ± 15. This set of six simplified SPM parameters describes 120 experimental CF energy levels with a relatively low *r.m.s.* value of 14.7 cm^{-1}. The CFPs B_{kq} corresponding to the $\hat{H}_{CF}$ form $C_2||z$ in Eq. (3) obtained from SPM using Eq. (8) are listed in column *Er-SPM* in Table 1. Note that in all tables below the following conventions are used for the entries: '-' denotes CFP not applicable for a given case, '0' denotes the actual zero value, while the numbers in brackets denote parameter values kept fixed in fittings.

In our comparative analysis of various fitting approaches, it is important to distinguish between the fittings based on the C(*complete*)-approach, which employs all 15 monoclinic CFPs B_{kq}, and the R(*reduced*)-approach, which employs only 14 independent CFPs out of the full monoclinic set [10,11]. The intrinsic features of monoclinic CFPs and the *actual* meaning of the R- and C-approach [10,11] have been elucidated in Refs. [11,21]. Usually, in the R-approach [10] the lowest rank monoclinic CFP ImB_{22} is 'reduced to', or rather just set to, zero for fittings. However, the common interpretation in literature of this *apparent* reduction as achieved by '*a suitable rotation of the axis system about the z-axis*' so not quite correct. In fact, prior to any R-approach fitting, no rotation is performed; here the *symbolic* [11] CFP ImB_{22} (or alternatively the monoclinic CFP ReB_{21} or ImB_{21}) is just neglected in fittings. The *actual* reduction to zero may take place only when dealing with the results of the C-approach, which return all 15 monoclinic CFPs. Then, a suitable rotation about the *nominal* [11] z-axis reduces ImB_{22} to zero, yielding the respective angle α. Importantly, no value of this angle can be obtained using the CFP sets fitted based on the R-approach. This additionally indicates the incorrectness of the common interpretation
discussed above.

Keeping in mind the above distinction between the C- and R-approaches, instead of randomly chosen starting CFPs in the R-approach, we rotate the CFP-SPM-C sets to obtain the corresponding CFP-SPM-R sets, which are then used as starting CFPs for fittings with ImB_{22}=0. Closeness of the CFP-SPM-R sets and the fitted CFP-Fit-R ones would ensure that after the back transformation to the full set corresponding to the C-approach by the reverse rotation $-\alpha/Oz$, CFP sets comparable to the CFP-SPM-C sets would be obtained. Using this procedure enables to increase reliability of the fitted CFP sets. As outlined in Introduction, extensive tests of various fitting approaches as well as transformations between CFP sets are indispensable for the proposed comprehensive procedure. Hence, in order to avoid confusion and facilitate comparisons between various resulting sets, a systematic labelling of CFP sets, namely, '*ion-set #-type-approach*' or '*ion-set #-type of transformation*' is adopted below.

In the second step, 15 CFPs B_{kq} (C-approach) were fitted to the experimental energy levels using the set *Er-SPM* in Table 1 as the starting set. This represents a specific constraint on the fitting procedure, namely, adoption of the same $\hat{H}_{CF}$ form (i.e. $C_2||z$) as arising from SPM calculations. Among CFPs, the 2nd-rank ones are usually the most difficult for accurate SPM determination, because they have the largest contributions from more distant ions [22]. Therefore, to explore the solution space for existence of various possible minima, a number of subsequent fittings were attempted based on scanning of the CF parameter space. The starting 2nd-rank CFPs were changed in different combinations from 500 to $-500\,cm^{-1}$ with a step of 50 cm^{-1}, whereas the 4th- and 6th-rank CFPs from the set *Er-SPM* in Table 1 were used as the starting values. So obtained CFPs set that yields the best minimum with *r.m.s.* value 14.1 cm^{-1} is given in column *Er-I-Fit-C* Table 1. Independently, fittings based on the R-approach yield the set *Er-I-Fit-R* in Table 1 with marginally better *r.m.s.* value 14.0 cm^{-1}. Additional fitting using 14 CFPs obtained first by the rotation of the set *Er-I-Fit-C* by −21.92° around the z-axis, which reduces ImB_{22} in this set to zero, yields the same CFP values as for the directly fitted set *Er-I-Fit-R*. This shows high reliability of the CFP sets fitted using independent approaches.

Interestingly, the scanning of the CF parameter space by changing the starting 2nd-rank CFP values resulted in two other minima with *r.m.s.* values only slightly worse than that resulting for the fitted set *Er-I-Fit-C* and *Er-I-Fit-R* (see Table 1). These two additional 15-CFP solutions (C-approach), distinguished

by the values of B_{20}=335 and $-513\,cm^{-1}$, are denoted below as *Er-II-Fit-C* and *Er-III-Fit-C*, respectively. After rotation around their respective *nominal* [11] *z*-axis by -5.52° and -9.95°, we obtain 14 CFPs (as in the R-approach) listed in column *Er-II-Fit-R* and *Er-III-Fit-R* in Table 1, respectively. These three CFP sets *Er-X-Fit-R* (*X*=*I*, *II*, *III*), obtained while adopting the same $\hat{H}_{CF}$ form ($C_2||z$) as arising from SPM calculations, are non-standard [10] and fall into different ranges of the CF parameter space [11]. Therefore the standardization procedure was carried out using the monoclinic sub-option in the CST computer package [25]; the set *Er-III-Fit-R* requires only change of signs of some CFPs. The standardized CFP sets (denoted: *ST*) corresponding to the three minima are listed in the last three columns *Er-X-ST* (*X*=*I*, *II*, *III*) in Table 1.

Interpretation of the standardized sets *Er-X-ST* (*X*=*I*, *II*, *III*) in Table 1 poses a dilemma. The values of the axial CFPs B_{k0} (k=2, 4, 6) and the rhombic 2nd-rank CFP ReB_{22} as well as those of the rotational invariants S_k and S, Eq. (7), are *seemingly* comparable with remarkable consistency. This might suggest that these multiple solutions are nearly equally good and, in a sense, 'equivalent' since they yield nearly the same energy levels, to within $<2\,cm^{-1}$ on average. However, careful comparative analysis of the transformation properties of the fitted CFP sets based on the monoclinic standardization approach and the multiple correlated fitting technique [10,11] reveals what follows. The $\hat{H}_{CF}$ form (see Eqs. (3)–(5)) corresponding to each fitted CFP set vary as indicated in Table 1. In general, the three possible monoclinic $\hat{H}_{CF}$ forms and the respective CFP sets are mutually transferable one into another, thus ensuring that each set would yield the same calculated energy levels. This option, if found valid for the sets *Er-X-ST* (*X*=*I*, *II*, *III*) in Table 1, would mean that such sets are the alternative correlated and physically equivalent sets [10,11]. However, the *apparent*, so partial, comparability of the sets in question runs counter this option. Hence, solution to the dilemma how to meaningfully interpret the multiple fitted CFP sets obtained in the following sections for the ion-host systems under consideration must be sought out elsewhere. For this purpose, below we first consider the sign interrelationships between monoclinic CFPs. This also helps us to provide solution to this dilemma in Section 3.2.

Importantly, for monoclinic symmetry sites there are 12 different choices of orientation of the axis system, leading to 12 different but equivalent CFP sets [26]. For comparative analysis, we present in Table 2 the additional alternative CFPs sets resulting from five monoclinic standardization transformations [10] applied to the set *Er-I-Fit-R*, taken as the initial set in its *nominal* axis system S1(x,y,z) [11], to S2(x,z,$-y$), S3(y,x,$-z$), S4(z,x,y), S5(y,z,x) and S6(z,y,$-x$), i.e. into other regions of the CF parameter space. Additional rotations of a given set Si by 180° around C_2 axis do not change CFPs. However, for the case $C_2||z$ other choices exist, which result from rotation of the set S1 by 90° and the set S3 by -90° around the *z*-axis and correspond to transformation: $(-y,x,z)\Rightarrow(y,-x,z)$ and $(-x,y,-z)\Rightarrow(x,-y,-z)$, respectively. This additional set S1′ [S3′] differs from S1 [S3] in signs of ReB_{22}, ReB_{42}, ImB_{42}, ReB_{62}, ImB_{62}, ReB_{66}, and ImB_{66}. For the case $C_2||y$, the rotation of the set S2 and S4 by 180° around the *x*-axis, which corresponds to transformation: $(x,-z,y)\Rightarrow(-x,z,y)$ and $(-z,x,-y)\Rightarrow(z,-x,-y)$, yields additional sets S2′ and S4′, respectively; they differ from the sets S2 and S4 by signs of ReB_{41}, ReB_{43}, ReB_{61}, ReB_{63}, and ReB_{65}. Similarly, for the case $C_2||x$ rotation of the sets S5 and S6 by 180° around the *y*-axis, which corresponds to $(y,-z,-x)\Rightarrow(-y,z,-x)$ and $(-z,y,x)\Rightarrow(z,y,x)$, yields additional sets S5′ and S6′, respectively; they differ from S5 and S6 only in signs of ImB_{42}, ImB_{43}, ImB_{61}, ImB_{63}, and ImB_{65}. These transformations yield in total 12 CFP sets corresponding to 12 different orientations of axis system that are possible for monoclinic symmetry. All these sets are equivalent, which means that they are characterized by the same values of the rotational invariants and yield the same CF energy levels after diagonalization of CF Hamiltonian. Each set can be transformed into each other by appropriate rotation of the axis system around the *x*-, *y*-, and/or *z*-axis.

Table 2
CF parameter sets (all with $\mathrm{Im}\,B_{22}$=0) obtained by monoclinic standardization transformations Si (i=1−6) of the CFP set *Er-I-Fit-R* in Table 1.

Set	*Er-I-Fit-R*≡*Er-S1*	*Er-S2*	*Er-S3*	*Er-S4*	*Er-S5*	*Er-S6*
$\hat{H}_{CF}$ form	$C_2\|\|z$	$C_2\|\|y$	$C_2\|\|z$	$C_2\|\|y$	$C_2\|\|x$	$C_2\|\|x$
Axis systems	$(x,y,z)=(-x,-y,z)$	$(x,z,-y)=(-x,-z,-y)$	$(y,x,-z)=(-y,-x,-z)$	$(z,x,y)=(-z,-x,y)$	$(y,z,x)=(-y,-z,x)$	$(z,y,-x)=(-z,-y,-x)$
B_{20}	170	342	170	−513	342	−513
ReB_{22}	−349	−279	349	71	279	−71
κ	−2.0	−0.82	2.0	−0.14	0.82	0.14
B_{40}	−360	−321	−360	−1034	−321	−1034
ReB_{41}	–	136	–	−158	–	–
ImB_{41}	–	–	–	–	−136	158
ReB_{42}	451	426	−451	−24	−426	24
ImB_{42}	32	–	32	–	–	–
ReB_{43}	–	−86	–	26	–	–
ImB_{43}	–	–	–	–	−86	26
ReB_{44}	−519	−551	−519	45	−551	45
ImB_{44}	−158	–	158	–	–	–
B_{60}	−201	124	−201	521	124	521
ReB_{61}	–	292	–	152	–	–
ImB_{61}	–	–	–	–	−292	−152
ReB_{62}	182	91	−182	163	−91	−163
ImB_{62}	87	–	87	–	–	–
ReB_{63}	–	52	–	−170	–	–
ImB_{63}	–	–	–	–	52	−170
ReB_{64}	−370	−283	−370	−177	−283	−177
ImB_{64}	162	–	−162	–	–	–
ReB_{65}	–	1	–	190	–	–
ImB_{65}	–	–	–	–	−1	−190
ReB_{66}	86	319	−86	61	−319	−61
ImB_{66}	233	–	233	–	–	–

Six additional equivalent sets (Si′, i=1−6) can be obtained by rotation of S1 by 90° and S3 by -90° around the *z*-axis, S2 and S4 by 180° around the *x*-axis as well as S5 and S6 by 180° around the *y*-axis (see text and Table 1); axis systems corresponding to the given CFP set are indicated.

Analogous alternative equivalent CFP sets exist also for the sets *Er-II-Fit-R* and *Er-III-Fit-R* in Table 1, so we refrain from providing them here. The physical insight arising from comparative analysis of Tables 1 and 2 is sufficient for our purpose as discussed below. It turns out that the sets *Er-II-ST* and *Er-III-ST* in Table 1 do not correspond to any of the 12 equivalent CFPs sets derived for the set *Er-I-Fit-R* and listed in Table 2. This means that it is not possible to transform the fitted CFP set *Er-I-Fit-R* into the set *Er-II-Fit-R* or *Er-III-Fit-R*, or vice versa, using any rotation of the axis system. Therefore, in spite of the pronounced, so partial, comparability, neither the three fitted sets *Er-X-Fit-C* nor the transformed sets *Er-X-Fit-R* and *Er-X-ST* (*X=I*, *II*, *III*) are mutually equivalent. Hence, these sets should be treated as corresponding to different minima. However, only one set may, hopefully, correspond to the global minimum, whereas then the other two sets must represent spurious solutions.

An important question arises: which of these three solutions should be treated as the most appropriate one. Two general criteria usually applied for choosing of the best experimentally determined CFP set are (see, e.g. in Refs. [13–16]) (i) goodness of the experimental energy level (and/or intensity) fittings measured, e.g. by the *r.m.s.* value and (ii) degree of correlation, i.e. closeness of the numerical values of the fitted CFPs and the starting CFPs obtained from model calculations using, e.g. superposition, angular overlap, and simple overlap models-succinctly overviewed in Ref. [27], or the exchange charge model [28]. For orthorhombic CFP sets, the latter criterion may be quantitatively assessed by the closeness factors C_{gl} and C_k [11] and norms ratios R_{gl} and R_k (k=2, 4, 6) [29] (modified in Ref. [30]), provided the sets being compared belong to the same region of CF parameter space. However, these quantities cannot be applied to CFP sets, which either belong to different regions of CF parameter space or correspond to different forms of $\hat{H}_{CF}$. This restricts application of the closeness factors and norms ratios only for some of the monoclinic (and triclinic) CFP sets considered below. In the case of incompatible CFP sets only their *apparent* closeness may be invoked based on an overall degree of correlation between the numerical CFP values.

The above criteria allow excluding from considerations the solution *Er-III-Fit-C* (*Er-III-Fit-R*), since the *r.m.s.* value is significantly larger than for two others. Also the closeness factors [11], which for {*Er-SPM*; *Er-III-Fit-C*} CFPs pair are C_{gl}=0.335, C_2=−0.556, C_4=0.571 and C_6=0.279, indicate the poor consistence of the CFP set obtained from the SPM step and that from the refined step. The *r.m.s.* values for the two remaining solutions of the type *C*: *Er-I-Fit-C* and *Er-II-Fit-C* (as well as the type *R*: *Er-I-Fit-R* and *Er-II-Fit-R*) are very similar: 14.1 and 14.3 cm^{-1} (14.0 and 14.2 cm^{-1}), respectively. However, the closeness factors for {*Er-SPM*; *Er-I-Fit-C*} CFPs pair are C_{gl}=0.914, C_2=0.908, C_4=0.947, C_6=0.843, whereas for {*Er-SPM*; *Er-II-Fit-C*} CFPs pair are C_{gl}=0.414, C_2=0.654, C_4=0.517, C_6=0.031, which points unambiguously to *Er-I-Fit* as the best solution. Thus, customarily one would accept the CFP set *Er-I-Fit-R* as the final set arising from CF analysis for Er^{3+} ions in $ErCl_3 \cdot 6H_2O$. However, this choice does not solve other important questions arising here, namely (i) Are there any physical reasons why such three different minima were obtained? (ii) Are these solutions simply accidental fitting minima?, and (iii) For which fitted CFP set its *nominal* AS may be assigned to the (*x*,*y*,*z*) axis system (Fig. 1) chosen for calculations of the starting CFPs *Er-SPM*. These questions will be dealt with in the next section.

3.2. Analysis of the multiple CFP solutions for Er^{3+} ions in $ErCl_3 \cdot 6H_2O$

It is generally expected that numerous local minima, often exhibiting comparable values of some, usually major, CFPs, may exist for low symmetry systems. Several examples of such minima may be encountered in literature, so usually numerical values are provided only for the 'final' selected CFP sets. The intriguing points arising from our analysis in Section 3.1 are (i) the obtained solutions are very similar in some respects (rotational invariants, the 2nd rank orthorhombic-like standardized CFPs, and the axial k=4 and 6 CFPs), and (ii) the general criteria invoked in literature are not sufficient to distinguish unambiguously between such numerically comparable fitted solutions.

As discussed in Section 3.1, the $\hat{H}_{CF}$ forms corresponding to the standardized CFP sets *Er-X-ST* (*X=I*, *II*, *III*) in Table 1 are different and cannot be transformed each into the other by any rotations of axis system. Thus these solutions turn out to be physically inequivalent and differ by orientation of their *nominal* ASs. However, the observed similarities strongly suggest that some sort of correlation exist between these sets. Importantly, in the approximated orthorhombic axis system, i.e. neglecting the monoclinic CFPs, these solutions would be almost equivalent. It is evidenced by the pronounced closeness existing between the 'pure' orthorhombic CFPs. The respective values calculated with only the orthorhombic CFPs for a given pair of two sets are C_{gl}=0.995 {*Er-I-ST* & *Er-II-ST*}, 0.996 {*Er-II-ST* & *Er-III-ST*}, and 0.996 {*Er-I-ST* & *Er-III-ST*}. Thus the observed differences between the sets *Er-X-ST* (*X=I*, *II or III*) are due to the fact that when the site symmetry is lowered from orthorhombic to monoclinic the C_2 axis becomes distinguished, while the other two axes in the plane perpendicular to the monoclinic axis (or direction) become arbitrary. Indeed, comparison of the fitted CFP sets in Table 1 with the equivalent sets obtained in Table 2 for the set *Er-I-Fit-R* reveals that, according to the nomenclature introduced for the orthorhombic-like 2nd-rank CFPs by Burdick and Reid [31], the set *Er-I-Fit-R* corresponds to the saddle point, *Er-II-Fit-R* to the maximal value of B_{20}, and *Er-III-Fit-R* to the minimal value of B_{20}.

The three solutions in Table 1 were obtained using the same starting values of B_{4q} and B_{6q} parameters, while probing different starting points for the 2nd-rank parameters. Therefore, one may expect that the ratio κ in Eq. (6) is an important factor responsible for the different minima returned by the fitting procedure. For a given orientation of the *nominal* AS for the case $C_2||z$, $C_2||y$, or $C_2||x$, the unique value of κ (see Table 2) characterizes each equivalent CFP set. Changes of this ratio, e.g. from $\kappa=-2.0$ to -0.82 for the set *Er-I-Fit-R*, corresponds to a rotation of the axis system from (*x*,*y*,*z*) (or (−*x*,−*y*,*z*)) to (*x*,*z*,−*y*) (or (−*x*,−*z*,−*y*)). Hence, it should be expected that changing the starting value of κ may lead to different minima, corresponding to the saddle point, maximal and minimal value of B_{20} (for the 2nd-rank orthorhombic-like CFPs). This is what is observed in our case. The rotational invariants for these minima should be the same; however, since the solutions correspond to different orientations of the *nominal* ASs, the $\hat{H}_{CF}$ forms should be also appropriately modified in order to obtain the equivalent CFPs sets.

Regardless of the difficulties in determination of reliable 2nd-rank CFPs using theoretical models (see, e.g. [13–15,27,28], the above considerations indicate that the starting κ values determined by a given model, play an important role in adopting a proper fitting procedure for CFPs of higher ranks. If this value is not adequate for the orientation of a given *nominal* AS, the subsequent fittings may results in CFPs obtained in another AS than initially assumed. In this regard, it seems advisable to explore the CF parameter space of possible solutions by changing the starting κ ratio. This, in general, should result in three minima, corresponding to three different orientations of AS. Comparison of the fitted 4th- and 6th-rank parameters with the starting ones, e.g. with the help of the closeness factors and norms ratios [11,29,30], should help in quantitative discrimination, out of several multiple solutions, of the fitted CFP set that has the

appropriate orientation of its *nominal* AS with respect to the AS initially assumed in the model calculations. These general intricacies inherent in the CFP fittings for monoclinic symmetry seem to be not widely realized in literature as yet.

For $\hat{H}_{CF}$ form chosen in a given way, e.g. $C_2||z$, four equivalent solutions with the same absolute κ value (see Table 2) should exist. Contrary to these expectations, three different values of $|\kappa|$ were obtained in our fittings performed with the $\hat{H}_{CF}$ ($C_2||z$) form. This additionally indicates that at least two solutions are spurious and should be treated as the local minima. However, the correlations discussed above that exist between these solutions, and particularly the fact that the 2nd-rank orthorhombic-like parameters of the sets *Er-II-Fit* and *Er-III-Fit* (Table 1) correspond very closely to the extreme points [31] of the set *Er-I-Fit* (Table 2), may suggest that some of these solutions represent only computational artifacts, presumably arising from choosing inappropriate $\hat{H}_{CF}$ form in the fitting procedure.

Thus, if these multiple minima are not just accidental but are correlated in a way, then consideration of properties of the fitted CFPs transformed into other regions of the CF parameter space, as done in Table 2, could help revealing their true origin. It was observed in our fittings that for each of the equivalent CFP sets in Table 2 derived for the set *Er-I-Fit-R*, there exist another non-equivalent CFPs set with similar absolute values but opposite signs of some CFPs, which yields almost identical calculated energy levels. Therefore, it is important to implement suitable fittings in order to consider variation of CFP sets fitted in different regions of CF parameter space with the changes of the signs of the starting CFPs. Such mutual correlations have proved to be helpful in gaining a better insight into the properties of monoclinic CFPs.

The above considerations and analysis of the CFP sets in Tables 1 and 2 have finally led us to the following interpretation of the multiple fitted CFP sets. This interpretation provides solution to the dilemma as well as answers to the questions presented in Section 3.1. We note that some of our fittings were based on the R-approach with the monoclinic 4th- and 6th-rank $\hat{H}_{CF}$ form that were inappropriate for the starting value of κ. It turns out that such fittings are equivalent to forcing the computer program used in our calculations [32] to fit the higher-rank CFPs to the values, which represent the closest values to the ones corresponding to the $\hat{H}_{CF}$ (starting) form appropriate for the starting κ value. In other words, the program attempts to find a fitted solution within the confines of the region represented by the 2nd-rank orthorhombic-like CFPs. This results in the monoclinic 4th- and 6th-rank CFPs adopting values close to those that would otherwise correspond to the appropriate $\hat{H}_{CF}$ form, i.e. one of the two other forms different from the $\hat{H}_{CF}$ (starting) form. However, then the higher-rank CFPs are assigned to the (k and q) labels fixed by the starting CFPs, i.e. the $\hat{H}_{CF}$ (starting) form, which in fact are inappropriate for the $\hat{H}_{CF}$ form corresponding to the appropriate region of the CF parameter space. This happens so since the program [32] can recognize neither the proper region of the CF parameter space nor the proper k and q labels; it can only output the CFP values that yield the lowest *r.m.s.* value.

In our fittings, fixing the $\hat{H}_{CF}$ (starting) form as for the case ($C_2||z$), the program locates also other 'second- or third-best' minima that correspond to the starting 2nd-rank CFPs located in other regions of the CF parameter space and thus corresponding to the case $C_2||x$ or $C_2||y$, while the 4th- and 6th-rank CFPs are confined to their counterparts still corresponding to the $\hat{H}_{CF}$ ($C_2||z$) form. Hence, such 'second- or third-best' minima, yet with the *r.m.s.* values very close to that for the 'best' minimum, must be considered as spurious and physically unacceptable minima. Importantly, these computer artifacts arise from the specific intricate features of monoclinic CFP sets, which have not been fully understood in literature as yet. To illustrate these intricate features and elucidate more convincingly the above interpretation of the fitted CFP sets, below we consider interrelationships between various fitted CFP sets and their alternative sets arising from additional test fittings and pertinent monoclinic standardization transformations.

In fact, in the framework of the multiple correlated fitting technique [10,11], fittings of monoclinic CFPs to experimental energy levels (and/or intensity) may be performed not only with the $\hat{H}_{CF}(C_2||z)$ form, which is the most common case, but also with the $\hat{H}_{CF}(C_2||x)$ or $\hat{H}_{CF}(C_2||y)$ form, in Eqs. (3)–(5). As discussed in Section 3.1, it is important to adhere consistently to a given $\hat{H}_{CF}$ form throughout all fittings. Let us consider, for example, this latter case. For the AS orientation corresponding to the case $C_2||y$, the sets *Er-S2* and *Er-S4* in Table 2 are equivalent to the set *I-Fit-R* in Table 1. Rotation of the set *Er-S2* or *Er-S4* by 180° around the *x*-axis yields two additional equivalent sets *Er-S2′* or *Er-S4′*. Each of those four equivalent CFPs sets may be used for fittings of experimental energy levels. For illustration, in Table 3 we present the results obtained from fittings based on the $\hat{H}_{CF}(C_2||y)$ form using several sets derived from the set *Er-S4* in Table 2 as the starting CFP sets, together with some related transformed sets.

As expected [10,11], the multiple correlated fittings starting from the equivalent sets *Er-S4* and *Er-S4′* yield the fitted CFPs differing only slightly from the starting ones—by no more than $3\,cm^{-1}$. Each fitted set *Er-S4-Fit* and *Er-S4′-Fit* can be subsequently transformed into the region corresponding to the $\hat{H}_{CF}(C_2||z)$ form by either S2 or S5 transformation. From the set *Er-S4-Fit* the transformation S2 $((z,x,y)=(-z,-x,y)\Rightarrow(-y,x,z)=(y,-x,z))$ yields the set *Er-S1′*, whereas S5 $((z,x,y)=(-z,-x,y)\Rightarrow(x,y,z)=(-x,y,z))$—the set *Er-S1* in Table 2. Analogously, the transformation S2 $((-z,x,-y)=(z,-x,-y)\Rightarrow(y,x,-z)=(-y,-x,-z))$ and S5 $((-z,x,-y)=(z,-x,-y)\Rightarrow(-x,y,-z)=(x,-y,-z))$ applied to the set *Er-S4′-Fit* yields the set *Er-S3* and *Er-S3′* in Table 2, respectively. Thus fitting with the $\hat{H}_{CF}(C_2||y)$ form yields, after appropriate transformation, four equivalent CFP sets (*Er-S1*, *Er-S1′*, *Er-S3* and *Er-S3′*) corresponding to the four possible orientation of the AS corresponding to the case $C_2||z$. This is an expected result, since for a well-defined minimum fittings in different regions Si of CF parameter space should yield equivalent CFP sets [33].

However, by changing the signs of ReB_{22}, ReB_{42}, ReB_{43}, ReB_{62}, ReB_{63} and ReB_{66} in the set S4 in Table 2 one may obtain a new CFP set *Er-S4″*, which describes the experimental energy levels with almost the same accuracy as the original set. Using the starting set *Er-S4″* yields the fitted CFPs shown in column *Er-S4″-Fit* in Table 3 with the *r.m.s.* value $14.2\,cm^{-1}$, which is larger by only $0.2\,cm^{-1}$ than the *r.m.s.* of *Er-S4-Fit*, while the same as *r.m.s.* of *Er-II-Fit-R* (Table 1). Another set *Er-S4‴* equivalent to *Er-S4″* can be obtained by rotation of *Er-S4″* by 180° around the *x*-axis, which corresponds to changing the signs of ReB_{41}, $Re\ B_{43}$, ReB_{61}, ReB_{63} and ReB_{65}. Similarly as for the pair *Er-S4″* & *Er-S4*, the set *Er-S4‴* differs from *Er-S4′* by the signs of ReB_{22}, ReB_{42}, ReB_{43}, ReB_{62}, ReB_{63} and ReB_{66}. Using the starting set *Er-S4‴* yields the fitted CFPs shown in column *Er-S4‴-Fit* in Table 3, again the *r.m.s.* value $14.2\,cm^{-1}$.

The transformation S2 or S5 applied to the fitted set *Er-S4″-Fit* or *Er-S4‴-Fit* yields four related CFP sets appropriate for the $\hat{H}_{CF}(C_2||z)$ form, one of which is presented in column *Er-S4″-Fit+TR/S5* in Table 3. Three other sets differ only by the signs of CFPs as indicated: *Er-S4″-Fit-S2*: ReB_{22}, ReB_{42}, ImB_{42}, ReB_{62}, ImB_{62}, ReB_{66} and ImB_{66}; *Er-S4‴-Fit-S2*: ReB_{22}, ReB_{42}, ImB_{44}, ReB_{62}, ImB_{64} and ReB_{66}; *Er-S4‴-Fit-S5*: ImB_{42}, ImB_{44}, ImB_{62}, ImB_{64} and ImB_{66}. These four transformed sets are equivalent and yield the same energy levels; they correspond to four possible orientations of the *nominal* AS for the case $C_2||z$. Additional fitting using the transformed set *Er-S4″-Fit+TR/S5* as the starting one based on

Table 3
CF parameter sets obtained from fittings based on the $\hat{H}_{CF}$ ($C_2||y$) form using the starting sets *Er-S4* (from Table 2) and *Er-S4′* (*Er-S4* rotated by 180°/Ox), and *Er-S4″*, *Er-S4‴*, and *Er-S2″* (obtained by changing in the sets *Er-S4*, *Er-S4′*, and *Er-S2* in Table 2, respectively, the signs of ReB_{22}, ReB_{42}, ReB_{43}, ReB_{62}, ReB_{63}, and ReB_{66}) as well as the sets transformed (*TR*/*Si*) by the transformation Si as indicated.

Starting set	*Er-S4*	*Er-S4′*	*Er-S4″*	*Er-S4‴*	NSS	*Er-S4″-Fit+TR/S5*	*Er-S2″*	*NSS*
$\hat{H}_{CF}$ form	$C_2\|\|y$	$C_2\|\|y$	$C_2\|\|y$	$C_2\|\|y$	$C_2\|\|z$	$C_2\|\|z$	$C_2\|\|y$	$C_2\|\|z$
Fitted or *TR* set	*Er-S4-Fit*	*Er-S4′-Fit*	*Er-S4″-Fit*	*Er-S4‴-Fit*	*Er-S4″-Fit+TR/S5*	*Er-S4″-Fit+TR/S5-Fit*	*Er-S2″-Fit*	*Er-S2″-Fit+TR/S5*
B_{20}	−512	−512	−513	−513	335	335	333	−513
ReB_{21}	[0]	[0]	[0]	[0]	–	–	[0]	–
ReB_{22}	70	70	−64	−64	−282	−282	283	62
ImB_{22}	–	–	–	–	0	[0]	–	0
κ	−0.14	−0.14	0.12	0.12	−0.84	−0.84	0.85	−0.12
B_{40}	−1034	−1034	−1031	−1031	−345	−352	−284	−1041
ReB_{41}	−159	159	−180	180	–	–	−67	–
ReB_{42}	−25	−25	47	47	376	382	−433	−46
ImB_{42}	–	–	–	–	129	129	–	−46
ReB_{43}	26	−26	−70	70	–	–	75	–
ReB_{44}	45	45	−2	−2	−561	−571	−566	67
ImB_{44}	–	–	–	–	−144	−144	–	−89
B_{60}	521	521	538	538	53	52	166	552
ReB_{61}	152	−152	125	−125	–	–	173	–
ReB_{62}	165	165	−184	−184	110	110	−76	260
ImB_{62}	–	–	–	–	306	306	–	92
ReB_{63}	−170	170	159	−159	–	–	115	–
ReB_{64}	−177	−177	−59	−59	−189	−189	−232	−129
ImB_{64}	–	–	–	–	−23	−23	–	−159
ReB_{65}	190	−190	239	−239	–	–	−8	–
ReB_{66}	60	60	−65	−65	371	371	−413	86
ImB_{66}	–	–	–	–	62	62	–	98
S_2	234	234	233	233	233	233	233	233
S_4	354	354	350	350	350	356	352	352
S_6	210	210	209	209	209	209	210	210
S	273	273	271	271	271	274	272	272
r.m.s.	14.0	14.0	14.2	14.2	–	14.2	14.7	–

No starting sets (NSS) exist for the transformed (*TR*) sets; for brevity the lines for CFPs: ImB_{21}, ImB_{41}, ImB_{43}, ImB_{61}, ImB_{63}, ImB_{65} which are not applicable for the cases indicated are omitted.

the $\hat{H}_{CF}(C_2||z)$ form yields the set *Er-S4″-Fit+TR/S5-Fit* in Table 3 that matches exactly the set *Er-II-Fit-R* in Table 1, which corresponds to the solution with the maximal value of B_{20}.

Analogous procedure can be applied to the sets *Er-S2* and *Er-S2′* in Table 2. By changing the signs of ReB_{22}, ReB_{42}, ReB_{43}, ReB_{62}, ReB_{63} and ReB_{66}, the new starting sets *Er-S2″* and *Er-S2‴* are obtained. Subsequent fittings to the experimental energy levels followed by the transformation S2 or S5 yield four equivalent sets, each corresponding to four possible orientations of the *nominal* AS for the case $C_2||z$, with $B_{20}=-513$ and $ReB_{22}=62$ or -62. Out of these solutions, the set *Er-S2″-Fit-S5* matches exactly the set *Er-III-Fit-R* in Table 1. The fitted set *Er-S2″-Fit* and its image transformed to the region S5, i.e. *Er-S2″-Fit+TR/S5*, are listed in the last two columns in Table 3. Note that using the starting set *Er-S2″* and *Er-S2‴* yields the *r.m.s.* value of 14.7 cm^{-1}, which is the same as obtained for the set *Er-III-Fit-R* in Table 1. Similarly, repeating the steps described above for the set *Er-S5* or *Er-S6* in Table 2, corresponding to the case $C_2||x$, yields the sets matching exactly the set *Er-II-Fit-R* or *Er-III-Fit-R* in Table 1, respectively.

Importantly, the series of fittings starting from different regions in the CF parameter space presented above shows that minima represented by the sets *Er-II-Fit* and *Er-III-Fit* in Table 1 may be obtained from fittings using the starting set *Er-I-Fit* transformed to other regions of CF parameter space with additional changes in signs of some parameters. This finding confirms our assertion that the two out of three different solutions obtained initially as described above represent in fact computer artifacts.

As discussed above, for monoclinic symmetry one may obtain 12 equivalent solutions resulting from 12 possible choices of AS. For the case $C_2||y$ and considering the solution *Er-I-Fit-R*, we have the set *Er-S2* with $\{B_{20}=342,\ ReB_{22}=-279\}$ and *Er-S4* with $\{B_{20}=-513,\ ReB_{22}=71\}$ in Table 2. Two other equivalent sets, *Er-S2′* and *Er-S4′* can be generated by 180° rotation around the *x*-axis which results in opposite signs of ReB_{41}, ReB_{43}, ReB_{61}, ReB_{63} and ReB_{65}. However, neither of the sets *Er-S2″*, *Er-S2‴*, *Er-S4″* or *Er-S4‴* used as the starting sets for fittings presented in Table 3, can be obtained by any transformation of *Er-S2*, *Er-S2′*, *Er-S4* or *Er-S4′*. The sets *Er-S2″*, *Er-S2‴*, *Er-S4″* or *Er-S4‴* are characterized by the same magnitudes of CFPs but differ in signs of ReB_{22}, ReB_{42}, ReB_{43}, ReB_{62}, ReB_{63} and ReB_{66} as compared with the sets *Er-S2*, *Er-S2′*, *Er-S4* or *Er-S4′*, respectively. For monoclinic case, a change in sign of these parameters occurs during the transformation of the *nominal* AS $(z,x,y)\Rightarrow(z,y,-x)$ or $(-z,x,-y)\Rightarrow(-z,y,x)$. This transformation, however, should be accompanied by modification of the $\hat{H}_{CF}$ form from the case $C_2||y$ to $C_2||x$. Consequently, ReB_{41}, ReB_{43}, ReB_{61}, ReB_{63}, and ReB_{65} for the sets *Er-S2″*, *Er-S2‴*, *Er-S4″* or *Er-S4‴* sets should by substituted by ImB_{41}, ImB_{43}, ImB_{61}, ImB_{63}, and ImB_{65}, respectively.

Thus the CFP values for the sets *Er-S4″* and *Er-S4‴* (with $B_{20}=-513$ and $ReB_{22}=-71\ cm^{-1}$) and those for the sets *Er-S2″* and *Er-S2‴* (with $B_{20}=342$ and $ReB_{22}=279\ cm^{-1}$) derived as described above from the sets in Table 3 should correspond to the case $C_2||x$ and not to $C_2||y$. If we substitute in the sets *Er-S2″*, *Er-S2‴*, *Er-S4″*, or *Er-S4‴* the CFPs ReB_{41}, ReB_{43}, ReB_{61}, ReB_{63}, and ReB_{65} by their imaginary counterparts, the subsequent fittings with the $\hat{H}_{CF}$ ($C_2||x$) form yield the sets *Er-S5*, *Er-S5′*, *Er-S6*, and *Er-S6′* in Table 2, which are equivalent with the set *Er-I-Fit-R* in Table 1.

The fact that goodness of fittings is not very sensitive to the signs of ReB_{22}, ReB_{42}, ReB_{43}, ReB_{62}, ReB_{63}, and ReB_{66} may suggest that the fitting program [32] does not differentiate properly

between the real ReB_{kq} and imaginary ImB_{kq} parts. If we accept $B_{20}=-513$ and $ReB_{22}=71\,cm^{-1}$ ($\kappa=-0.14$) as values of the 2nd-rank CFPs appropriate for fittings in the region S4 or S4′ (the case $C_2||y$), than the fittings with $B_{20}=-513$ and $ReB_{22}=-71$ ($\kappa=0.14$) should be performed for the $\hat{H}_{CF}(C_2||x)$ form (*Er-S6* or *Er-S6′* in Table 2). However, if one attempts fittings using the $\hat{H}_{CF}(C_2||y)$ form, which is not appropriate for this κ value, the least-squares procedure within the fitting program [32] is forced to search for solutions with such ill-imposed initial conditions. Hence, the lowest minimum is returned by ascribing blindly the values of ImB_{kq} (as it should be if one used the proper $\hat{H}_{CF}(C_2||x)$ form) to their real counterparts, thus yielding the solutions *Er-S4″-Fit* or *Er-S4‴-Fit*. Actually the three minimal solutions presented in Table 1 were obtained for the $\hat{H}_{CF}(C_2||z)$ form. This case corresponds exactly to the situation described above, but with the fittings carried out using, e.g. the starting set *Er-S4″* or *Er-S4‴* (the case $C_2||y$) additionally transformed to the region S2 or S5 (the case $C_2||z$).

The above reasoning reveals that if one would used the $\hat{H}_{CF}$ form appropriate for the given value of κ, than the solution *Er-II-Fit-R* in Table 1 (with $B_{20}=335\,cm^{-1}$ and $ReB_{22}=-282\,cm^{-1}$) would correspond not to the case $C_2||z$ but to the case $C_2||y$. As a consequence, we would obtain a solution identical with that presented in column *Er-S2* in Table 2, equivalent with the set *Er-I-Fit-R* in Table 1. Similarly, when using the $\hat{H}_{CF}$ form appropriate for the value of $\kappa=-0.83$ (the case $C_2||y$), the set *Er-S4* in Table 2 would be obtained instead of the spurious set *Er-III-Fit-R* in Table 1.

The above considerations were carried out assuming provisionally that the set *Er-I-Fit-R* in Table 1 is our final solution appropriate for the case $C_2||z$. This solution was selected on the basis of the values of *r.m.s.* and the closeness factors and norms ratios. Obviously, if one assumes that the set *Er-II-Fit-R* or *Er-III-Fit-R* in Table 1 is the solution appropriate for the case $C_2||z$, the above reasoning would be still valid. In any case, an important conclusion is that the three *apparently* different minima listed in Table 1 could hypothetically represent equivalent solutions had the $\hat{H}_{CF}$ form adopted for each case been appropriate for a given set of the starting CFPs.

Another important outcome of our considerations is that in the CFP fittings for monoclinic symmetry one may unknowingly obtain CFPs set for different orientations of the *nominal* AS than implicitly assumed, i.e. although the starting CFP values correspond to the $\hat{H}_{CF}(C_2||z)$ form and this form is used in fittings, the fitted CFP values may turn out to correspond to the $\hat{H}_{CF}(C_2||x)$ or $\hat{H}_{CF}(C_2||y)$ form. Various reasons may be responsible for such unexpected solutions; we name a few below.

Inappropriate fitted CFP sets may result from the calculation procedure used, possibly due to some modifications of the starting parameters, e.g. changing the 2nd-rank CFP values—as exemplified by our calculations and fittings described above. This may lead to spurious minima. As shown above, to avoid selecting spurious minima as the final CFP sets, analysis of the sensitivity of fitted CFPs to changes in the signs of the starting CFPs may be helpful. For a given orientation of the *nominal* AS, only the starting CFPs with the value of κ confined in a certain range (see Section 2) will converge during fittings into the minimum solution that is characteristic for the assumed orientation of the *nominal* AS. It is also possible that even without CFP modifications, the starting 2nd-rank CFPs may be not evaluated with sufficient accuracy for the assumed orientation of the *nominal* AS, thus resulting in the fitted CFPs corresponding to another *nominal* AS.

Another reason for appearance of spurious minima, i.e. CFP sets with values appropriate for the $\hat{H}_{CF}(C_2||x)$ or $\hat{H}_{CF}(C_2||y)$ form, which may be unknowingly so erroneously assigned to the case $C_2||z$, may arise from inaccurate energy levels analysis involving CFP sets expressed in different axis systems taken from various sources or obtained by different methods. Such cases require special care to be taken concerning the transformation properties of CFP sets. This may occur particularly when the descent in symmetry method is applied for initial evaluation of the starting CFPs, while the approximated higher symmetry axes do not coincide with the actual symmetry axes. In the next sections we consider illustrative examples of such erroneous CFP calculations for Ln^{3+} ions in $LnCl_3\cdot 6H_2O$ systems revealed by our literature search.

3.3. Energy level calculations and fittings of free-ion and CFPs for Tm^{3+} ions in $TmCl_3\cdot 6H_2O$

Based on the arguments presented in Sections 3.1 and 3.2 for the case of Er^{3+} ions in $ErCl_3\cdot 6H_2O$, we have accepted the set *Er-I-Fit-C* in Table 1 as the final CFP solution, whereas the orientation of the *nominal* AS in which this set is expressed as coinciding with the (*x*,*y*,*z*) axis system (Fig. 1) chosen for the SPM calculations of the starting set *Er-SPM*. In this section we consider the case of Tm^{3+} ions in $TmCl_3\cdot 6H_2O$ along the lines used for of Er^{3+} ions in $ErCl_3\cdot 6H_2O$ in Section 3.1. These considerations should provide an additional check of the validity of the choices made for the latter case. It is interesting to verify whether the spurious minima analogous to those obtained for Er^{3+} ions, which resulted from assignment of an erroneous $\hat{H}_{CF}$ form to a given *nominal* AS, also are encountered in fittings of the energy levels for Tm^{3+} ions. Moreover, the specific features of the two lowest levels of Tm^{3+} enable direct determination of the orientation of the *nominal* AS, in which the final CFP solution is expressed with respect to the crystallographic axes, on the basis of the calculated eigenvectors. This complementary method to that used in the case of Er^{3+} ions in $ErCl_3\cdot 6H_2O$, namely, comparison of the fitted CFP sets with the SPM derived CFP set is discussed in Section 3.5.

We have attempted fittings of Tm^{3+} energy levels using the $\hat{H}_{CF}$ form for the case $C_2||z$ and the three solutions obtained for Er^{3+} in Table 1 as the starting CFPs. The best and second best minimum with the *r.m.s.* value of 11.2 and $11.4\,cm^{-1}$ was obtained for the starting set *Er-I-Fit-R* and *Er-I-Fit-C*, respectively. Fittings with the starting sets *Er-II-Fit-R* and *Er-III-Fit-R* resulted in worse minima, with the *r.m.s.* values of 12.2 and $12.0\,cm^{-1}$, respectively. The three solutions characterized by the lowest *r.m.s.* values are listed in Table 4. Fitting using the C-approach [10] result as the starting set (after appropriate rotation of the *nominal* AS) yields exactly the same CFPs as those obtained in the direct R-approach. To reduce ImB_{22} in the set *Tm-I-Fit-C* to zero, the rotation around the *z*-axis by -29.56° is required.

3.4. Analysis of the multiple CFP solutions for Tm^{3+} ions in $TmCl_3\cdot 6H_2O$

In order to analyze the distinction between the sets in Table 4 and their origin, we provide the results of transformations of the set *Tm-I-Fit-R* (taken as *Tm-I-S1*) to the region S2, S4, and S6 [10] in Table 5. In the case of Tm^{3+} we may conclude that, although the set *Tm-III-Fit-R* in Table 4 does not correspond to the extreme points [31] of B_{20} (for the 2nd-rank orthorhombic-like CFPs) in the set *Tm-I-Fit-R*, the origin of the set *Tm-II-Fit-R* seems to be of the same nature as elucidated for the sets *Er-II-Fit-R* i *Er-III-Fit-R*. This can be easily evidenced by calculations analogous to those carried out for Er^{3+} in Section 3.2. The starting set *Tm-S1+TR/S4‴* (obtained by changing the signs of ReB_{22}, ReB_{42}, ReB_{62} and ReB_{66} in the set *Tm-S1+TR/S4* in Table 5) used for fitting with the $\hat{H}_{CF}(C_2||y)$ form yields the set *Tm-S4‴-Fit* in Table 5. This CFP set describes the experimental energy levels almost as accurately as the

Table 4
CF parameters for Tm^{3+} ions in $TmCl_3 \cdot 6H_2O$ obtained from fittings of the energy levels [4] using various starting CFP sets (see text).

Starting set	*Er-I-Fit-R*	*Er-I-Fit-C*	*Er-III-Fit-R*
Fitted set	*Tm-I-Fit-R*[a]	*Tm-I-Fit-C*	*Tm-III-Fit-R*
B_{20}	114	114	154
ReB_{22}	−345	−177	351
ImB_{22}	0	−296	0
B_{40}	−528	−528	−590
ReB_{42}	420	111	−414
ImB_{42}	122	423	−169
ReB_{44}	−337	−247	−280
ImB_{44}	459	−514	−391
B_{60}	−124	−124	−106
ReB_{62}	24	35	−75
ImB_{62}	−26	7	111
ReB_{64}	−182	18	−8
ImB_{64}	77	−197	−254
ReB_{66}	218	−203	−123
ImB_{66}	−302	312	−316
S_2	224	224	232
S_4	381	382	367
S_6	169	170	177
S	273	274	271
r.m.s.	11.2	11.4	12.0

For brevity the lines for the real and imaginary parts of CFPs B_{21}, B_{41}, B_{43}, B_{61}, B_{63}, B_{65}, which are not applicable for the cases indicated are omitted.

[a] For this fit the free-ion parameters were determined as (all values in cm^{-1}): E_{avg}=18060(2), F^2=102089(32) , F^4=72009(108), F^6=51669(85), and ζ_{4f}=2526(1), while other parameters were kept constant as follows [18]: α=19.25, β=−665.0, γ=1936, M^0=4.93, M^2=2.76, M^4=1.87, P^2=730, P^4=548, P^6=365. For other fitted CFP sets practically the same free-ion parameters were obtained within the uncertainties for the respective parameters, so we refrain from listing them here. The *Tm-I-Fit-R* fitted set can be also obtained from the set *Tm-I-Fit-C* by rotation around the *z*-axis by −29.56°.

original set; its *r.m.s.*=11.5 cm^{-1} is larger by only 0.3 cm^{-1} than *r.m.s.* for the set *Tm-S4-Fit*.

Subsequent transformation S2 applied to the set *Tm-S4‴-Fit* yields the set *Tm-S4‴-Fit-TR/S2* in Table 5, which corresponds to the $\hat{H}_{CF}(C_2||z)$ form. Additional fitting using the latter set as a starting set based on the $\hat{H}_{CF}$ $(C_2||z)$ form yields the set matching exactly the set *Tm-II-Fit-R* in Table 4. Thus the origin of the spurious minimum *Tm-II-Fit-R* is the same as that figured out for the Er^{3+} sets. Such spurious solutions arise from the usage of the fixed $\hat{H}_{CF}$ form, which in two cases is inappropriate for the region of the starting CFPs, as judged by comparison of the CFP set obtained by SPM in the well-defined axes and that obtained in the *nominal* axes of a given starting set. Change of signs of ReB_{22}, ReB_{42}, ReB_{62} and ReB_{66} in the set *Tm-S1+TR/S4* corresponds to transformation $(z,x,y)=(-z,-x,y)$ $\Rightarrow (z,y,-x)=(-z,y,x)$ and should be accompanied by substituting ReB_{41}, ReB_{43}, ReB_{61}, ReB_{63} and ReB_{65} parameters by ImB_{41}, ImB_{43}, ImB_{61}, ImB_{63}, and ImB_{65}, respectively, in order to obtain the $\hat{H}_{CF}$ form appropriate for the case $C_2||x$. This modified CFP set is identical with the set *Tm-S1+TR/S6′* in Table 5, which after the transformation S6 matches exactly the set *Tm-I-Fit-R*.

Thus similarly as in the case of Er^{3+}, the spurious minimum *Tm-II-Fit-R* arises from wrong assignment of the *nominal* axis system with respect to the CAS (or the modified CAS*, as appropriate). For $LnCl_3 \cdot 6H_2O$ the monoclinic axis is parallel to the crystallographic *b*-axis. Let us assume tentatively (to be confirmed in the next section), that the *nominal* AS (*x*,*y*,*z*), in which the set *Tm-I-Fit-R* is obtained, is related to the modified CAS* (*a**,*b*,*c*) defined in Section 3.1 as *x*=*c*, *y*=*a**, and *z*=*b*||C_2. Hence, our simulation was performed assuming the AS $(-z,x,-y)$ for the set *Tm-S4‴-Fit*, and consequently the set *Tm-II-Fit-R* was then obtained, after the transformation S2, in the *nominal* AS $(y,x,-z)$. It turns out, however, that for the set *Tm-S4‴-Fit* the AS $(-z,y,x)$ should be assigned, and thus the transformation S2 would lead to the AS (y,z,x). Hence, although, the solution *Tm-II-Fit-R* was obtained with the $\hat{H}_{CF}(C_2||z)$ form, the *z*-axis of its *nominal* AS is not parallel to the axis *b*||C_2; actually in this AS: *x*=*b*, *y*=*c*, and *z*=*a**. Thus, the actual fitting leading to the set *Tm-II-Fit-R* was performed in the region S4 or S6 for the case $C_2||x(b)$, which corresponds to the monoclinic axis perpendicular to the crystallographic *b*-axis, which is in contradiction to the real crystal structure. Obviously, as it has been shown by simulations performed for Er^{3+} ions, the set *Tm-II-Fit-R* can be also obtained in fittings performed in the region S2 or S5 for the case $C_2||y$. However, these choices also correspond to an erroneous adoption of the monoclinic axis in the $\hat{H}_{CF}$ form used, i.e. $(C_2||z)$, with respect to the actual C_2 axis. Thus the two minima in Table 4 were obtained with the $\hat{H}_{CF}$ form appropriate for the case $C_2||z$, but with different orientation of the *nominal* AS with respect to the CAS*, i.e. with $C_2||b$ and $C_2 \perp b$.

3.5. Alternative method for determination of the orientation of the nominal axes for Tm^{3+} ions in $TmCl_3 \cdot 6H_2O$

We note that in the case of the fittings of energy levels measured by non-directional techniques [11], any fitted CFP set may be assigned only to a *nominal* AS. Correlation of a given *nominal* AS with the well-defined axes in crystal may be determined only indirectly via comparison with the CFP sets calculated using one of the CFP models (see, e.g. [13–15,27,28]). This method, namely, comparison of the fitted CFP sets with the SPM derived CFP set was used in the case of Er^{3+} ions in $ErCl_3 \cdot 6H_2O$. The fact that for $TmCl_3 \cdot 6H_2O$ the direction of magnetization axis with respect to the crystallographic axes (CAS and thus CAS*) is known [12] enables direct correlation of the axis system (AS) chosen for the CF analysis with the crystallographic structure. This complementary method requires consideration of relations between the magnetic properties and the eigenvectors of Tm^{3+} ions in $TmCl_3 \cdot H_2O$.

We utilize here the specific features of the two lowest levels Z_1 and Z_2 of Tm^{3+}, which are nearly incidentally degenerate. As a result, the splitting of these two levels in the external magnetic field may be observed and the orientation of the magnetic vector with respect to the crystallographic axes may be established [12]. The magnetic moment μ in $TmCl_3 \cdot 6H_2O$ is found [12] to be perpendicular to the twofold symmetry C_2 axis aligned along the crystallographic *b*-axis. The crucial fact is that the Zeeman splitting factor of the Tm^{3+} levels Z_1 and Z_2 is the largest if the *z*-axis of the *nominal* AS of the fitted CFPs (or the *symbolic* AS assigned to the *symbolic* CFPs in $\hat{H}_{CF}$ [11]) is aligned along μ. Hence, the eigenvectors calculated using a given fitted (or *symbolic*) CFP set, which contain the largest fraction of the $|J=6, M_J=\pm 6>$ states will correspond to the maximum value of the Zeeman splitting. This enables to find the *nominal* ASs corresponding to the fitted CFP set that matches the orientation of $\boldsymbol{\mu}$, which itself is well defined relative to the CAS (CAS*).

In order to apply the above method, the CFP set *Tm-I-Fit-C* in Table 4 was transformed from the axis system (*x*,*y*,*z*) to (*z*,*x*,*y*), thus putting the *z*-axis into the plane of μ moment. Then, we rotated the new AS around the *y*-axis searching for the highest fraction of $|J=6, M_J=\pm 6>$ components in the eigenvectors of the levels Z_1 and Z_2. This maximum, with the $|M_J=\pm 6>$ percentage of 98.6%, was achieved after rotation around the *y*-axis by −21.5°. The eigenvector components for the levels Z_1 and Z_2 are $|Z_1> = -0.702|M_J=6> -0.043|M_J=4> -0.064|M_J=3> +0.022|M_J=1> +0.024|M_J=0> -0.022|M_J=-1> +0.064|M_J=-3> -0.043|M_J=-4> +0.702|M_J=-6>$ and $|Z_2> = 0.703|M_J=6> -0.043|M_J=4> -0.065|M_J=3> +0.010|M_J=1> +0.010|M_J=-1> -0.065|M_J=-3> +0.043|M_J=-4> -0.703|M_J=-6>$. The CFP set corresponding to this AS orientation (with the *z*-axis along $\boldsymbol{\mu}$ and the *y*-axis parallel to the monoclinic axis) is given in column *Tm-I-Fit-μ* in Table 5.

Table 5
CF parameter sets obtained by monoclinic transformations S2, S4, and S6 of the set *Tm-I-Fit-R* in Table 4.

Set	*Tm-I-Fit-R*≡*Tm-S1*[a]	*Tm-S1+TR/S2*	*Tm-S1+TR/S4*	*Tm-S1+TR/S6*	*Tm-S4‴-Fit*	*Tm-S4‴-Fit+TR/S2*	*Tm-I-Fit-μ*[b]
$\hat{H}_{CF}$ form	$C_2\|\|z$	$C_2\|\|y$	$C_2\|\|y$	$C_2\|\|x$	$C_2\|\|y$	$C_2\|\|z$	$C_2\|\|y$
Axis system	$(x,y,z)=(-x,-y,z)$	$(x,z,-y)=(-x,-z,-y)$	$(z,x,y)=(-z,-x,y)$	$(z,y,-x)=(-z,-y,-x)$	*nominal*	*nominal+TR/S2*	*nominal+TR/S2*[b]
B_{20}	114	365	−480	−480	−498	335	−464
ReB_{21}	–	0	0	–	[0]	–	−297
ImB_{21}	–	–	–	0	–	–	–
ReB_{22}	−345	−242	103	−103	−70	270	19
ImB_{22}	[0]	–	–	–	–	0	–
B_{40}	−528	−218	−882	−882	−613	−354	−544
ReB_{41}	–	−472	386	–	−604	–	−630
ImB_{41}	–	–	–	−386	–	–	–
ReB_{42}	420	224	−196	196	−46	−210	−101
ImB_{42}	122	–	–	–	–	−454	–
ReB_{43}	–	48	−276	–	−257	–	−214
ImB_{43}	–	–	–	−276	–	–	–
ReB_{44}	−337	−596	−40	−40	−84	−301	−234
ImB_{44}	459	–	–	–	–	−474	–
B_{60}	−124	−56	389	389	253	−231	−144
ReB_{61}	–	−237	−304	–	290	–	361
ImB_{61}	–	–	–	304	–	–	–
ReB_{62}	24	210	−68	68	201	−143	196
ImB_{62}	−26	–	–	–	–	−202	–
ReB_{63}	–	178	73	–	198	–	−6
ImB_{63}	–	–	–	73	–	–	–
ReB_{64}	−182	−164	−45	−45	−41	−170	13
ImB_{64}	77	–	–	–	–	−237	–
ReB_{65}	–	−99	−8	–	42	–	−76
ImB_{65}	–	–	–	8	–	–	–
ReB_{66}	218	129	82	−82	55	32	36
ImB_{66}	−302	–	–	–	–	−168	–
S_2	224	224	224	224	227	227	224
S_4	381	381	381	381	374	374	382
S_6	169	169	169	169	176	176	170
S	273	273	273	273	272	272	274
r.m.s.	11.2	–	–	–	11.5	–	–

The set *Tm-S4‴-Fit* results from fitting with the $\hat{H}_{CF}$ ($C_2||y$) form using the starting set *Tm-S4‴* obtained by changing the signs of ReB_{22}, ReB_{42}, ReB_{62} and ReB_{66} in the set *Tm-S4*, and the set *Tm-S4‴-Fit+TR/S2* from transformation S2 of the fitted set *Tm-S4‴-Fit*.

[a] *Tm-S1+TR/S3* ($\hat{H}_{CF}$ ($C_2||z$) form, $(y,x,-z)=(-y,-x,-z)$) can be obtained from the set *Tm-S1* by changing the signs of ReB_{22}, ReB_{42}, ImB_{44}, ReB_{62}, ImB_{64} and ReB_{66} parameters; *Tm-S1+TR/S5* ($\hat{H}_{CF}$ ($C_2||x$) form, $(y,z,x)=(-y,-z,x)$) can be obtained from the set S2 by changing the signs of ReB_{22}, ReB_{41}, ReB_{42}, ReB_{61}, ReB_{62}, Re_{65} and ReB_{66} parameters and substituting ReB_{kq} by ImB_{kq} for q=odd. Six additional equivalent sets (*Tm-S1+TR/Si′*, $i=1-6$) can be obtained by rotation of *Tm-S1* by 90° and *Tm-S1+TR/S3* by −90° around the *z*-axis, *Tm-S1+TR/S2* and *Tm-S1+TR/S4* by 180° around the *x*-axis, whereas *Tm-S1+TR/S5* and *Tm-S1+TR/S6* by 180° around the *y*-axis.

[b] Set *Tm-I-Fit-C* in Table 4 transformed from the axis system (*x*,*y*,*z*) to (*z*,*x*,*y*) and rotated around the new *y*-axis by −21.5°; this set is related to the magnetic moment ($\boldsymbol{\mu}$) considered in details in Section 3.5.

To achieve the AS orientation corresponding to the set *Tm-I-Fit-μ* (with the *z*-axis along $\boldsymbol{\mu}$), the CAS* used to obtain the starting CFPs for Er^{3+} using SPM model (Section 3.1), should be transformed from the AS (*x*,*y*,*z*) to (*z*,*x*,*y*) and then rotated by −27.6° around the new *y*-axis. Note that a different assignment of the CAS* was used in Refs. [4] and [5] as compared with that in our case (see Section 3.1); in Refs. [4] and [5] the direction of the μ vector is located at 60° relative to the crystallographic *c*-axis, whereas in our notation this angle is −30° (see, Fig. 1). Thus the correspondence between the axis systems, in which the starting CFPs and the fitted CFPs are expressed, is fairly good, their mutual orientation differs by rotation by about 6° around the *z*-axis. This proves our assumption that the *nominal* AS for the solution *Tm-I-Fit-R* corresponds to the AS with the *z*-axis parallel to the monoclinic axis (i.e. the crystallographic *b*-axis). Thus, the CFP set *Tm-I-Fit-R* matches best the observed direction of the magnetic moment $\boldsymbol{\mu}$ in $TmCl_3 \cdot 6H_2O$ and may be considered as most suitable set consistently describing the optical and magnetic properties. Hence, this set should be treated as the final result of our CF calculations for Tm^{3+} in $TmCl_3 \cdot 6H_2O$.

In short, the considerations in Sections 3.1–3.4, concerning the origin of the spurious minima encountered in the extensive CF calculations presented above, reveal deeper problems pertaining to the intricate features of the fitted CFP sets and inadequate procedure for their analysis. These problems are not merely computational problems, and if unrealized may lead to serious pitfalls. One may find in pertinent literature several examples (see, e.g. [5,6]) of inadvertent usage of such misleading procedure for analysis of energy levels and the fitted CFP sets for RE^{3+} ions in various ion-host systems. Particularly, the simulations presented above convincingly reveal the hitherto unrealized pitfalls in the procedure applied by Olsen et al. [5] for determination of CFPs for Tm^{3+} ions in $TmCl_3 \cdot 6H_2O$, which has lead to the spurious minimum adopted as the final solution.

3.6. Derivation of CF parameters for Er^{3+} and Tm^{3+} by descent in symmetry method

In the CF calculations of the energy levels for Tm^{3+} in $TmCl_3 \cdot 6H_2O$ Olsen et al. [5] used the idea of a higher symmetry approximation, i.e. assuming the existence of a sixfold axis of rotation coinciding with the magnetic axis of the crystal (perpendicular to the actual monoclinic axis). The CF Hamiltonian expressed in the axis system with the *symbolic z*-axis [11] along the sixfold rotational axis contains only four non-zero CFPs: B_{20}, B_{40}, B_{60} and ReB_{66}. The procedure used in Ref. [5] was as follows. In the first step the values of these four B_{kq} were determined using

fittings of the experimentally determined pseudo-levels, defined as the C_2 symmetry CF levels grouped into degenerate levels expected for the transitions allowed for the higher C_{6v} symmetry. In the next step the additional 11 CFPs required for symmetry reduced from C_{6v} to C_2 were considered and degeneracy of pseudo-levels was lifted. The fittings of experimental levels were performed, and then the fitted CFPs were transformed to the axis system with the z-axis along the actual monoclinic C_2 axis. In this axis system the final fittings of experimental energy levels were performed yielding the CFPs reported in Ref. [5].

To compare these CFPs with other literature data, the CFPs [5] were converted by us from the original Stevens to Wybourne notation [34,35] and rotated around the z-axis by the angle of -28.5° in order to reduce ImB_{22} to zero, yielding the CFPs (in cm^{-1}): $B_{20}=152$, $ReB_{22}=346$, $B_{40}=-640$, $ReB_{42}=-433$, $ImB_{42}=36$, $ReB_{44}=-286$, $ImB_{44}=-134$, $B_{60}=-91$, $ReB_{62}=-146$, $ImB_{62}=124$, $ReB_{64}=-49$, $ImB_{64}=-283$, $ReB_{66}=-210$, and $ImB_{66}=-230$. This final CFP set obtained by Olsen et al. [5] (denoted here as *Olsen-I*) corresponds closely to the set *Tm-II-Fit-R* obtained in our analysis (Table 4). The closeness factors for the pair of CFP sets {*Olsen-I*; *Tm-II-Fit-R*} are $C_{gl}=0.9397$, $C_2=1.0000$, $C_4=0.9263$ and $C_6=0.9480$. Some differences may result from different computer programs used by Olsen et al. [5] and by us. In the program [32] used in our calculations, the entire matrix combining the free-ion and CF interactions is simultaneously diagonalized, whereas it seems that the authors [5] did not calculate the absolute values of the energy levels by diagonalization of the free-ion Hamiltonian and rather calculated CF splittings relative to the center of gravity of the free-ion multiplets. Indeed, using our program a refitting with the starting set *Olsen-I* yields exactly the set *Tm-II-Fit-R*, so with the *r.m.s.* value 12.0 cm^{-1}, i.e. larger than 11.2 cm^{-1} obtained for our best fit set *Tm-I-Fit-R*. This indicates that a local minimum rather than the global one was achieved in Ref. [5].

It seems that Olsen et al. [5] have not taken a sufficient care about transformation properties of the monoclinic CF Hamiltonian. For the system under consideration only one actual monoclinic $C_2||b$ axis exists (Fig. 1). Consequently, only for the choice of the *nominal* (or *symbolic*) AS with $z||b$, the $\hat{H}_{CF}$ ($C_2||z$) form is appropriate. To lift the degeneracy of the pseudo-levels Olsen et al. [5] employed 11 CFPs appropriate for the $\hat{H}_{CF}$ ($C_2||z$) form, prior to transformation of the AS to such orientation that the z-axis is along the actual twofold symmetry axis. In view of the interpretation of the multiple fitted CFP sets provided in Section 3.2, this procedure is unfortunately faulty. Note that the solution obtained in Ref. [5] is exactly the same as our set *Tm-II-Fit-R* in Table 4 obtained when we forced the program to fit the parameter values to the $\hat{H}_{CF}(C_2||z)$ form instead to that appropriate for the case $C_2||x$ or $C_2||y$. Actually, in the AS with the z-axis taken along the magnetic axis, the z-axis is perpendicular to the actual monoclinic axis. Then one should use the $\hat{H}_{CF}$ form for the case $C_2||x$ or $C_2||y$, i.e. the additional 11 CFPs introduced at the descent in symmetry step should appropriately be taken as in Eqs. (4) or (5), respectively.

Olsen et al. [5] noticed that spectroscopic splitting factors calculated using the eigenvectors obtained from their fittings are inconsistent with experimental data and concluded that '*the calculated fit was in a coordinate system with the z-axis along μ and perpendicular to the twofold symmetry axis of the crystal*'. Consequently, to align properly the z-axis with respect to the C_2 axis at the Ln site, they performed appropriate rotation of the axis system. This is a correct procedure, however, the authors [5] did not realize the fact arising directly from their conclusion, namely, that in such a case, the fitting carried out before transformation, i.e. using parameters appropriate for the $\hat{H}_{CF}(C_2||z)$ form, was incorrect. Moreover, transformation of the axis system from that with the z-axis perpendicular to the monoclinic axis to the system with the z-axis parallel to the monoclinic axis should be accompanied by an appropriate change of the $\hat{H}_{CF}$ form, which was not implemented in the fittings [5].

We have repeated Olsen et al. [5] calculations using the proper procedure. Our fit performed with the starting CFPs appropriate for the C_{6v} approximated symmetry yields (in cm^{-1}): $B_{20}=-454$, $B_{40}=-1262$, $B_{60}=291$, and $B_{66}=192$, i.e. close to the CFPs reported in Ref. [5]: $B_{20}=-508$, $B_{40}=-1024$, $B_{60}=320$ and $B_{66}=153$. Comparison of these values with those in Table 5 indicates that the appropriate choice of the axis system is that for the case $C_2||y$. Thus, in the next, descent in symmetry step, we have included in our calculations monoclinic CFPs appropriate for the case $C_2||y$, i.e. as in Eq. (5). Subsequently, the 15 fitted CFPs were transformed to the axis system for the case $C_2||z$ and the final fits to the experimental energy levels [5] were carried out. This procedure yields the *r.m.s.* = 11.4 cm^{-1} and CFPs identical with those of the fitted set *Tm-I-Fit-C* in Table 4.

Alternatively, one may assume that an approximate C_2 axis exists along the magnetic moment, perpendicular to the actual twofold axis parallel to the b-axis. This, however, corresponds to the approximate orthorhombic symmetry case, and the CF Hamiltonian should contain only nine CFPs: B_{20}, ReB_{22}, B_{40}, ReB_{42}, ReB_{44}, B_{60}, ReB_{62}, ReB_{64} and ReB_{66}. After the first step, analogous to that described above, all orthorhombic CFPs were fitted to the experimental data [5], in the axis system with the z-axis along the magnetic axis. Subsequently, the resulted CFP set was transformed to the AS with the z-axis along the actual twofold axis and rotated by -30°. This transformation results in 15 CFPs appropriate for monoclinic C_2 symmetry. Final fittings using this CFP set as the starting one yield again CFPs identical with those of the fit *Tm-I-Fit-C* with the *r.m.s.* value of 11.4 cm^{-1}.

Couture and Rajnak [6] analyzed the energy levels of Er^{3+} ion in $ErCl_3 \cdot 6H_2O$ using approximate D_{4d} symmetry. In this case there are only three axial CFPs: B_{20}, B_{40} and B_{60}. The approximate eightfold inverse symmetry axis lies in the crystallographic ac-plane, i.e. it is perpendicular to the actual monoclinic axis. The authors [6] obtained CFPs as (in cm^{-1}) $B_{20}=-531\pm12$, $B_{40}=-1075\pm30$ and $B_{60}=712\pm28$. They have also presented CFPs transformed to the case $C_2||z||b$ and suggested that their CFPs could be used as the starting parameters in the C_2 symmetry fittings. However, in the AS with the axis $z||b$ it is more difficult to discuss the deviation from the D_{4d} symmetry. For this purpose, it is better to compare the D_{4d} CFPs with our CFPs transformed to the region S4 or S6 (Table 2). Indeed, the values of axial CFPs obtained in our analysis, i.e. the set *Er-S4* or *Er-S6* in Table 2, are very close to those obtained by Couture and Rajnak [6]. The values of the non-axial CFPs in these sets may serve as a measure of departure from D_{4d} with lowering symmetry. Since the axial 2nd- and 4th-rank CFPs are dominant, the D_{4d} symmetry may be considered as a good approximation. However, for the 6th-rank CFPs the contributions from lower symmetry CF components are significant and some of them constitute almost 40% of B_{60} value as indicated by comparison of the values of B_{6q} and B_{60} in the sets *Er-S4* or *Er-S6* in Table 2.

Thus, although the D_{4d} symmetry approximation seems to be good to start with, subsequent fittings should be performed with some care. In particular, a direct fitting using as starting the D_{4d} axial CFPs obtained by Couture and Rajnak [6] transformed to the AS for the case $C_2||z||b$ yields a minimum worse than that obtained by us. The largest differences are observed for the 6th-rank CFPs, for which the adoption of the starting zero values seems to be the worst option. Therefore, it is advisable to apply procedure analogous to that used above for Tm^{3+}. We assume that the AS chosen for the D_{4d} symmetry approximation corresponds to the case $C_2||y$ (with $y||b$). Thus, after initial

refinement of the three axial D_{4d} symmetry CFPs, in the next step of calculations we have included the monoclinic CFPs appropriate for the case $C_2||y$, i.e. as in Eq. (5). Since the 2nd- and 4th-rank non-axial CFPs are expected to be small, we kept them at zero and optimized initially only B_{20}, B_{40}, and all 6th-rank CFPs. In a subsequent step, 14 CFPs were optimized with only ImB_{22} kept at zero. This procedure yields CFP set identical with the set *Er-S4* in Table 2.

Thus, the descent/ascent in symmetry approach may be useful in analysis of low symmetry systems provided that enough care is taken concerning the transformation properties of CFPs. Importantly, the same final CFPs are obtained in the step-wise fittings based on the descent in symmetry approach as in the direct fittings employing the starting CFP sets derived from SPM calculations based on the actual lower site symmetry. In view of the potential existence of various local minima for low symmetry cases, the fact that two independent fitting methods did yield the same fitted CFPs proves additionally the reliability of the resulting CFP sets.

4. Summary and conclusions

The hydrated lanthanide (Ln) trichlorides have served as one of the first crystalline hosts for studies of the spectroscopic properties of the Ln^{3+} ions [3–6]. However, the lack of a systematic variation of CFPs along the lanthanide series as well as the existence of the non-standard CFPs in the literature have motivated us to re-analyze the CF splittings of Ln^{3+} ions in $LnCl_3 \cdot 6H_2O$ systems. As a follow-up on the results obtained earlier for Ho^{3+} ions in $HoCl_3 \cdot 6H_2O$ [9], in this paper we have re-analyzed crystal-field splittings of Er^{3+} ions in $ErCl_3 \cdot 6H_2O$ and Tm^{3+} ions in $TmCl_3 \cdot 6H_2O$. This analysis provides consistent and standardized crystal-field parameter (CFP) sets. Experimental energy levels obtained by other authors [3–6] were fitted to Hamiltonian parameters representing the combined free-ion and crystal-field interactions for Er^{3+} and Tm^{3+} ions in $LnCl_3 \cdot 6H_2O$. The reliable starting values of the CFPs were obtained from superposition model calculations based on the actual monoclinic C_2 symmetry of the Ln sites. The values of six free-ion parameters and CF parameters for the three equivalent forms of monoclinic CF Hamiltonian considered, namely, 15 CFPs (the C-approach) or 14 CFPs (the R-approach), were refined and the energy level structure was simulated yielding a number of CFP sets.

Analysis of the multiple solutions obtained in this way, which exhibit relatively low and quantitatively comparable *r.m.s.* deviation, poses a dilemma that turns out to arise from intricate aspects of fitted CFPs for low site symmetry systems. In order to elucidate these intricate aspects and hence to solve this dilemma we utilized a comprehensive procedure consisting in (i) model calculations of CFPs, (ii) scanning of the CF parameter space using values of the starting 2nd-rank CFPs in reasonable ranges, (iii) using starting CFP sets located in different regions of the CF parameter space for fittings, (iv) considering the effect of sign changes in CFPs on the fitted solutions, and (v) comparative analysis of the transformation properties of all fitted CFP sets based on the monoclinic standardization approach and the multiple correlated fitting technique. An important finding arising from our analysis is a convincing indication that some of the multiple and *seemingly* comparable solutions for fitted CFP sets turn out to be spurious.

Elucidation of the nature of these computer artifacts requires consideration of problems inherently involved in usual fitting procedures. Some of the fitted CFP sets, among the multiple comparable solutions, turn out to correspond to the *nominal* axis systems [11] with the *x*- or *y*-axis *apparently* parallel to the monoclinic axis, even if the starting CFPs were expressed in the axis system with the *z*-axis taken along the monoclinic axis. Importantly, it turns out that such *apparently* correlated fitted solutions cannot be transformed one into another, which indicates that two out of three such solutions must represent computer artifacts. Question arises what criteria can help us to find out the spurious solutions. The latest version of the fitting program used in our calculations, unlike its previous versions, does not contain any internal constraints on monoclinic (or triclinic) CFPs and the forms of monoclinic CF Hamiltonian; fittings may be carried out using any of the maximum 27 CFPs. Nevertheless, caution is needed since by inappropriate choice of input CFPs users may unknowingly force the fitting program into calculations that are bound to result in some computer artifacts appearing among multiple solutions for CFP sets.

In practice, identification of such spurious solutions is especially difficult and it seems likely that some of the reported CFP sets may fall into this category. However, it is of outmost importance to distinguish them from the physically valid CFP sets, which exhibit similar quality as measured by the *r.m.s.* values. Such artifacts may most likely occur when the descent in symmetry method is applied for initial evaluation of the starting CFPs, while the approximated higher symmetry axes do not coincide with the actual symmetry axes. Wider applications of the proposed procedure in CF studies of low site symmetry systems may improve the reliability of the CFP sets reported in literature. Reliable CFP sets are indispensable to unravel any trends that may exist in variation of CFPs across the lanthanide series. Further studies on other Ln^{3+} ions in $LnCl_3 \cdot 6H_2O$ hydrates as well as other systems are needed to verify the CFP values and hence to establish such trends.

Acknowledgments

This work was partially supported by the Research Grant from the Polish Ministry of Science and Tertiary Education in the years 2006–2010.

References

[1] B.G. Wybourne, Spectroscopic Properties of Rare Earths, Interscience, New York, 1965.
[2] G.H. Dieke, Spectra and Energy Levels of Rare Earth Ions in Crystals, Interscience, New York, 1968.
[3] I.H. Harrop, J. Chem. Phys. 42 (1965) 4000.
[4] J. Stöhr, D.N. Olsen, J.B. Gruber, J. Chem. Phys. 55 (1971) 4463.
[5] N. Olsen, J. Stöhr, J.B. Gruber, J. Chem. Phys. 55 (1971) 4471.
[6] L. Couture, K. Rajnak, Chem. Phys. 85 (1984) 315.
[7] K. Binnemans, C. Görller-Walrand, J. Alloys Compd 250 (1997) 326.
[8] W.T. Carnall, P.R. Fields, R. Sarup, J. Chem. Phys. 54 (1971) 1476.
[9] M. Karbowiak, C. Rudowicz, P. Gnutek, A. Mech, J. Alloys Compd 451 (2008) 111.
[10] C. Rudowicz, J. Chem. Phys. 84 (1986) 5045.
[11] C. Rudowicz, J. Qin, J. Lumin. 110 (2004) 39.
[12] D.N. Olsen, J.B. Gruber, J. Chem. Phys. 54 (1971) 2077.
[13] J. Mulak, Z. Gajek, The Effective Crystal Field Potential, Elsevier, Amsterdam, 2000.
[14] D.J. Newman, B. Ng, Rep. Progr. Phys. 52 (1989) 699.
[15] D.J. Newman, B. Ng (Eds.), Crystal Field Handbook, Cambridge University Press, Cambridge, 2000.
[16] A. Mech, Z. Gajek, M. Karbowiak, C. Rudowicz, J. Phys. Condens. Mat. 20 (2008) 385205.
[17] W.T. Carnall, H. Crosswhite, H.M. Crosswhite, J.P. Hessler, N.M. Edelstein, J.G. Conway, G.V. Shalimoff, R. Sarup, J. Chem. Phys. 72 (1980) 5089.
[18] Ch. Görller-Walrand, K. Binnemans, Rationalization of crystal-field parametrization, in: K.A. Gschneidner Jr., L.R. Eyring (Eds.), Handbook on the Physics and Chemistry of Rare-Earths, vol. 23, Elsevier, North-Holland, Amsterdam, 1996 (Chapter 155).
[19] C. Rudowicz, Chem. Phys. 97 (1985) 43.
[20] N.C. Chang, J.B. Gruber, R.P. Leavitt, C.A. Morrison, J. Chem. Phys. 76 (1982) 3877.
[21] C. Rudowicz, J. Qin, Phys. Rev. B 67 (2003) 174420.

[22] D.J. Newman, B. Ng, Superposition model, in: D.J. Newman, B. Ng (Eds.), Crystal Field Handbook, Cambridge University Press, 2000, pp. 83–119.
[23] M. Marezio, H.A. Pletinger, W.H. Zacharisen, Acta Cryst. 4 (1961) 234.
[24] R.D. Rogers, L.K. Kurihara, Lanthanide Actinide Res. 1 (1986) 296.
[25] C. Rudowicz, Computer package CST: conversions, standardization and transformations, in: D.J. Newman, B. Ng (Eds.), Crystal Field Handbook, Cambridge University Press, 2000, pp. 259–268.
[26] P. Gnutek, C. Rudowicz, Opt. Mater. 31 (2008) 391.
[27] P. Porcher, M. Couto Dos Santos, O. Malta, Phys. Chem. Chem. Phys. 1 (1999) 397.
[28] B.Z. Malkin, in: A.A. Kaplyanskii, R.M. Macfarlane (Eds.), Spectroscopy of Solids Containing Rare-earth Ions, North-Holland, Amsterdam, 1987, pp. 13–50 (Chapter 2).
[29] C. Rudowicz, P. Gnutek, M. Karbowiak, Phys. Rev. B 76 (2007) 125116.
[30] C. Rudowicz, P. Gnutek, M. Lewandowska, M. Orłowski, J. Alloy. Compd 467 (2009) 98.
[31] G.W. Burdick, M.F. Reid, Mol. Phys. 102 (2004) 1141.
[32] M.F. Reid, F-shell Empirical Programs, University of Canterbury, New Zealand, 1984.
[33] C. Rudowicz, M. Chua, M.F. Reid, Physica B 291 (2000) 327.
[34] C. Rudowicz, Magn. Reson. Rev. 13 (1987) 1;
C. Rudowicz, Magn. Reson. Rev. 13 (1988) 335 Erratum.
[35] C. Rudowicz, S.K. Misra, Appl. Spectr. Rev. 36 (2001) 11.